A very first real data application of

Stochastic wave-equation based AVO inversion of seismic pre-stack data

by

Omar C. Rivera-Herrera

to obtain the degree of Master of Science

at the Delft University of Technology,

to be defended publicly on Friday August 21, 2020 at 14:00 hrs.

Student number:	4783573	
Project duration:	March 1, 2020 – August 7, 2020	
Thesis committee:	Prof. Dr. Ir. Kees Wapenaar,	TU Delft, Academic Supervisor
	Prof. Dr. Ir. Dries Gisolf,	Delft Inversion, Supervisor
	Prof. Dr. Ir. Ranajit Ghose,	TU Delft
	Prof. Dr. Ir. Ernst Niederleithinger,	RWTH Aachen

This thesis is confidential and cannot be made public until September 1st, 2020.

TU Delft

The work in this thesis was made in collabortation with Delft Inversion and Shell. The MSc in Applied Geophysics is a joint effort among TU Delft, ETH Zutich and RWTH Aachen:

MSc Applied Geophysics
IDEA League
Faculty of Civil Engineering & Geosciences
Delft University of Technology

Supervisors: Prof. Dr. Ir. Dries Gisolf
Prof. Dr. Ir. Kees Wapenaar
Dr. Ir. Peter Haffinger
Dr. Ir. Raphic Van Der Weiden

ABSTRACT

Wave-Equation-Based Amplitude Vs Offset (WEB-AVO) inversion solves the full elastic wave equation both for properties and for the total wavefield. It is a non-linear inversion technique that accounts for multiple scattering and mode conversions inside the target interval. When prior geological information interpreted from well logs is incorporated, stochastic inversion can be performed by honouring Bayes' theorem for probability density functions. The posterior function is proportional to the product of the likelihood function and the prior probability density function.

The prior probability function is built from well logs and is a complex mixture of Gaussians that account for thicknesses, property values and their corresponding standard deviations.

The likelihood function is built from the maximum likelihood estimator, the result of the deterministic inversion, and from the Hessian derived from the inversion kernel, scaled by the variance of the noise in the data.

The present work proposes that the best estimate of the noise in the data can be extracted from the residual of the seismic-to-well match. The inaccuracy of the method can be quantified by taking the second derivative of the posterior function at the Maximum a Posteriori estimate. The present work also proposes that an additional source of inaccuracy is the intrinsic uncertainty, or non-uniqueness, of the method. It can be estimated with the help of random starting models on a perfect data set (synthetic data).

The stochastic WEB-AVO inversion is a natural extension of the already existing deterministic WEB-AVO inversion workflow. The inversion result is constrained by the prior to honour the true geology observed in the wells.

ACKNOWLEDGEMENTS

The applied geophysics master program is a great journey of academic and personal growth. Advises, insights, opinions and encouragements from many people have contributed to the development of this master thesis project.

I would like to thank the Delft Inversion team for all the generous help and support provided during, and even before, the master thesis project. I send a word of gratitude to Peter Haffinger and Panos Doulgeris for opening the opportunity for a student like me to collaborate in such a great team. I also thank Nick, Mengmeng, Pablo and Hansel for all his support and help throughout the duration of the master project. I will be forever thankful to Dries Gisolf, my main supervisor, for his daily instructions, energy and willingness to share his enormous experience and knowledge with me, I look up to you.

I would like to thank Kees Wapenaar, my academic supervisor, for his helpful insight and for his readiness to provide guidance throughout all the project.

This project wouldn't have been able to exist without the help of our partner Shell R&D who kindly provided real data for the research and expertise from different specialists. I would like to thank Raphic Vander Weiden, Fons Ten Kroode and Marc Bevaart for his invaluable insight and knowledge shared during multiple online session.

Not only has Shell been a partner for the Master thesis, but I was a recipient of the Idea League full comprehensive scholarship provided by Shell. Thank you.

I would like to thank my applied geophysics colleagues, I could always feel their friendship and support all along the way.

A special word of gratitude goes to my parents Omar and Cecilia, because I owe them everything, and to my siblings Zeltzin, Daniel and Benjamin, they have always been a source of strength, inspiration and guidance for me.

Finally, I would like to thank CONACyT, the National Council of Science and Technology of Mexico for helping young students like me in their academic formation providing academic, moral and financial support.

CONTENTS

Introduction 1

1 CHAPTER 1:STOCHASTIC WEB–AVO INVERSION 5
- 1.1 WEB-AVO Inversion . . . 5
- 1.2 Stochastic Inversion . . . 7
  - 1.2.1 Bayes' theorem . . . 7
  - 1.2.2 Maximum a Posteriori Estimate . . . 8
- 1.3 Prior probability density function . . . 9
  - 1.3.1 Layer-based model vs Grid-based model . . . 10
- 1.4 Likelihood function . . . 11
  - 1.4.1 Estimate of the noise in the data . . . 12
  - 1.4.2 Estimate of the uncertainty of the method (WEB-AVO inversion) . . . 12
- 1.5 Posterior probability density function . . . 13
  - 1.5.1 Minimization of the objective function . . . 13

2 CHAPTER 2: METHODOLOGY 15
- 2.1 Well interpretation: Prior Model Creation . . . 15
- 2.2 Seismic-to-well tie: wavelet extraction and data noise estimation . . . 18
- 2.3 Deterministic Inversion: parameter tuning and choice of the target interval . . . 19
  - 2.3.1 Background Model . . . 19
  - 2.3.2 Parameter tuning . . . 19
  - 2.3.3 Target interval . . . 19
- 2.4 Random realisations: method uncertainty estimation . . . 20
- 2.5 Stochastic Inversion: single location and 2D section . . . 20

3 CHAPTER 3: CASE STUDY 21
- 3.1 Presentation of the study case . . . 21
- 3.2 Prior building: well interpretation . . . 22
  - 3.2.1 Well 2 Interpretation . . . 22
  - 3.2.2 Well 1 and 3 interpretation . . . 26
- 3.3 Seismic-to-Well tie . . . 27
- 3.4 Deterministic WEB-AVO Inversion at well location . . . 31

4 CHAPTER 4: RESULTS AND DISCUSSION 35
- 4.1 Likelihood function building: Looking for the noise in the data . . . 35
- 4.2 Stochastic Inversion at well locations . . . 37
- 4.3 Stochastic inversion using grid-based mean as starting model . . . 42
- 4.4 Random realisations . . . 43
- 4.5 2D section deterministic and stochastic inversion . . . 46

5 CONCLUSIONS 51

LIST OF FIGURES

Figure 1.1 Deterministic WEB-AVO inversion workflow. 6
Figure 1.2 Stochastic WEB-AVO inversion workflow. 6
Figure 1.3 Schematic representation of Bayes' theorem using Gaussian functions as probability density functions. 8
Figure 1.4 Weight matrix 2D representation. It depicts the probability of every grid point i to be sitting in the layer j. 11
Figure 2.1 Well interpretation example on creating a blocky layered model from Gamma ray, compressional velocity, shear velocity and density logs. 16
Figure 2.2 Gaussian distribution for a layer with negative thickness. . . . 17
Figure 3.1 Relative location of wells 1, 2 and 3. These wells were carefully selected to test stochastic WEB-AVO inversion on a section crossing all three wells. The wells are deviated, and the cyan lines represent a surface projection of the trajectory of the wells. 22
Figure 3.2 Well 1 displaying target interval where units have been interpreted inside every formation. 23
Figure 3.3 Well 2 displaying target interval where units have been interpreted inside every formation. 23
Figure 3.4 Well 3 displaying target interval where units have been interpreted inside every formation. 24
Figure 3.5 Gaussian distribution for the fluvial formation, the red area is 60% of the total curve integral, it is the probability that the layer is not existent. During the building of the prior the red area is replaced by a proportional delta function at x=0. The blue area represents the probability of the layer existing. The average value of the layer is 15 m. 26
Figure 3.6 Well 2 with predicted values in missing intervals and with a 300 m extension of salt, the red curves are the smooth versions of the logs and the black lines are the interpreted units of the prior. 28
Figure 3.7 Well 1, the red curves are the smooth versions of the logs and the black lines are the interpreted units of the prior. 28
Figure 3.8 Well 3, the red curves are the smooth versions of the logs and the black lines are the interpreted units of the prior. 29
Figure 3.9 Seismic-to-well tie at location of well 2. The panels show the seismic data, the matched Kennett synthetics generated from the smooth logs and the residual. 29
Figure 3.10 Result of the seismic-to-well tie. 30
Figure 3.11 WEB-AVO inversion results from Kennett generated synthetic data. The black curves are the smooth true logs, the blue curves are the inverted properties and the red curves are the background. The three panels on the right show the seismic data, the predicted synthetic data based on the inverted parameters and the residual. 31
Figure 3.12 Regularization: Compressibility κ issued from inversion of the seismic data with different number of CG steps. The black curves are the smooth true logs, the blue curves are the inverted properties and the red curves are the background. . 32

Figure 3.13 Regularization: Compressibility κ issued from inversion of the seismic data with different sparse gradient weight values. The black curves are the smooth true logs, the blue curves are the inverted properties and the red curves are the background. 33

Figure 3.14 WEB-AVO deterministic inversion results from the seismic data at location of well 2. The black curves are the smooth true logs, the blue curves are the inverted properties and the red curves are the background. The three panels of the right show the seismic data, the modelled seismic data with the inverted parameters and the residual. 34

Figure 4.1 Stochastic inversion results with different values for the variance of the noise in the data. The black curves are the smooth true logs, the blue curves are the inverted properties and the red curves are the background. 36

Figure 4.2 WEB-AVO stochastic inversion with optimal parameters and a variance of 0.01. The black curves are the smooth true logs, the blue curves are the inverted properties and the red curves are the background. The three panels on the right show the seismic data, the predicted synthetic data based on the inverted parameters and the residual. 37

Figure 4.3 Deterministic inversion results comparison between the logs-derived background and the grid-based-derived background. Both background have the same frequency content, a low-ass filter has been applied (4-6 Hz). The black curves are the smooth true logs, the blue curves are the inverted properties and the red curves are the background. 38

Figure 4.4 Stochastic inversion results comparison between the logs-derived background and the grid-based-derived background. Both backgrounds have the same frequency content, a low-pass filter has been applied (4-6 Hz). The black curves are the smooth true logs, the blue curves are the inverted properties and the red curves are the background. 39

Figure 4.5 Deterministic and stochastic inversion results comparison at well 1 location using the background derived from the grid-based mean. The black curves are the smooth true logs, the blue curves are the inverted properties and the red curves are the background. 40

Figure 4.6 Deterministic and Stochastic inversion results comparison at well 3 location using the background derived from the grid-based mean. The black curves are the smooth true logs, the blue curves are the inverted properties and the red curves are the background. 41

Figure 4.7 Deterministic inversion results that compare the use of the background starting model vs using the grid-base mean as a starting model at well two location. 42

Figure 4.8 Stochastic inversion results that compare the use of the background as starting model vs using the grid-base mean as a starting model at well 2 location. 43

Figure 4.9 Histograms for four κ grid-points for 100 random realisation sampled from the prior. 44

Figure 4.10 Histograms of the inversion results using the 100 random realisations as the starting model. The 'True value' is the grid-point value from the smooth wells and the 'Value no contrast' is the result of the inversion using the background as starting model. 45

Figure 4.11 Assessment of the uncertainty of the inversion method on synthetic data. The green curve is the standard deviation computed from the random realisations for every grip-point. 45
Figure 4.12 Assessment of the global uncertainty incorporating the uncertainty of the inversion in the seismic data. The green curve is now the uncertainty estimated from the posterior and it incorporates the uncertainty of the method. 46
Figure 4.13 Near offset of the 2D section. Well 3 is located at the extreme left and well 1 is located at the extreme right. 47
Figure 4.14 Comparison of deterministic inversion vs stochastic inversion for κ over the 2D line going from well 3 to well 2 and from well 2 to well 1. The units are m^2/N. 48
Figure 4.15 Comparison of deterministic inversion vs stochastic inversion for M over the 2D line going from well 3 to well 2 and from well 2 to well 1. The units are m^2/N. 49

INTRODUCTION

In recent years, the energy sector has been facing challenges to image the earth's deepest internal structure. The understanding of how the subsurface has been built up over geologic time is vital for the development of facilities that aim to extract resources or simply aim to understand the earth's natural processes.

Imaging the earth's interior relies on the reflection seismic method. Seismic reflection surveys are widely used and are a well-known geophysical technique [Kearey et al., 2002]. The "current state of sophistication" has been reached as a result of developments made by the Oil and Gas industry and recent advances in electronics and computing technology.

The current development of seismic reflection methods allows to perform surveys inland and offshore, reaching targets from several tens of meters depth up to several thousands.

Processing and interpretation of reflection images become more valuable after one or several wells have been drilled and logged. The interpreter can then identify the real lithology and rock type of the reflectors. Once the identification has been made at the well location, seismic can provide a 'remarkably accurate' mapping of the lithology over a certain distance away from the well. [Claerbout, 1985].

The method relies on the following principles: seismic waves are transmitted into the subsurface and they are reflected at the interfaces where there are changes in the elastic properties of the earth. The arrival times corresponding to events are measured. A first primary objective is usually to map depth, dip and strike of the reflectors and their lateral variability [Sheriff, 2002].

We can define a seismic wave as a "disturbance through a compressible or elastic medium generated by some mechanical wave motion" [Liner, 2016], energy is then transferred from one region to another but there is no transfer of mass. The efficiency of energy transport is governed by the elastic properties of the materials. These parameters are essential to build a numerical model of the underground materials. Another primary goal in exploration seismology is to estimate these parameters from observed data.

When building a numerical model, we must make the difference between a 'forward problem' and an 'inverse problem'. In the first case, the physical properties of a system are known, one can then compute the response of the system to a known stimulus [Oliver et al., 2008]. In reflection seismology, the physical properties are the elastic properties of the rocks, the response of the system is the seismic data.

For a linear problem, the following equation for the forward model can be defined.

$$\mathbf{d} = \mathbf{G}\mathbf{m} \tag{0.1}$$

where $\mathbf{d}$ is the calculated data, $\mathbf{m}$ is the known model vector and $\mathbf{G}$ is called the "sensitivity matrix", or kernel, relating $\mathbf{d}$ and $\mathbf{m}$.

On the other hand, the inverse problem involves the determination of plausible physical properties of the system when one is given the response of the system to the known stimulus. In the case of an over-determined system, where the size of $\mathbf{d}$ is greater than the size of $\mathbf{m}$, we can find a solution of the inverse problem in the least squares sense, from:

$$\mathbf{m} = \left(\mathbf{G}^T\mathbf{G}\right)^{-1}\mathbf{G}^T\mathbf{d} \tag{0.2}$$

In this case $\mathbf{m}$ is the estimated model vector and $\mathbf{d}$ is the observed data. The inversion of the square matrix $\mathbf{G^TG}$ will often need to be stabilised.

Elaborating further, seismic inversion is the method of retrieving the rock properties that match the acquired field data [Sheriff, 2002]. The classical approach for high resolution seismic reservoir characterisation over a target interval relies on the basic one-dimensional convolutional model [Russell, 1988]: a seismic trace is the convolution of two functions, the earth's primary reflectivity series in the arrival-time domain and the seismic source function. This approach relies on the assumption of linearity of the earth's response in terms of the primary reflectivities [Tarantola, 1984]. However, the solution of the full elastic wave equation that governs the propagation of seismic waves is not linear in the primary reflectivities, but also contains multiple internal reflections and mode-conversions [Pratt, 1999] [Virieux and Operto, 2009].

Delft Inversion has developed a commercial wave-equation-based amplitude-variation-with-offset inversion (WEB-AVO) that solves the full elastic wave equation for the total wave-field, while inverting the measured data for the material properties. This non-linear inversion method accounts for all internal multiple scattering and mode conversion over the target interval [Gisolf and M. van den Berg, 2010] [Gisolf et al., 2017].

Applications of WEB-AVO inversion have been applied successfully in different domains like reservoir characterization [Gisolf et al., 2017], quantitative estimation of injected CO_2 in the context of carbon capture storage [Haffinger et al., 2018] and some other challenging real case study characterizations of subsurface properties [Beller et al., 2015], [Haffinger et al., 2015], [Barajas-Olalde et al., 2019], [Contreras et al., 2019], [Dhelie et al., 2019].

The present work aims to test the existing WEB-AVO inversion in a real case study setting and to extend it to a stochastic approach by incorporating prior geological information from well data..

For the definition of the stochastic extension of WEB-AVO inversion, an assessment of the noise in the data must be performed. This parameter controls the width of the so called 'likelihood function' in Bayes' Rule. The uncertainty of the result of the stochastic inversion must also include the uncertainty of the method, not captured by the width of the likelihood function. A careful assessment of the uncertainty, or non-uniqueness, of the inversion must be carried out.

Three primary objectives are targeted in the present project:

- Estimate the noise in the data
- Analyse effect of using prior information on the WEB-AVO inversion results
- Estimate uncertainty, or non-uniqueness, of the inversion with the help of ensembles of starting models

In the first chapter a quick overlook of WEB-AVO inversion is presented and the principles of stochastic inversion are treated in detail.

In the second chapter, the methodology followed for this thesis will be explained.

In the third chapter, the real-data case study provided by Shell will be presented. Special attention will be given to the construction of the 'prior geological model probability density distribution' and the 'likelihood function'.

Finally, in the fourth chapter, the results of the stochastic inversion and the uncertainty assessments will be presented and discussed.

1 CHAPTER 1:STOCHASTIC WEB-AVO INVERSION

The aim of the present work is to test the stochastic extension of the deterministic WEB-AVO inversion. Therefore, a quick overview of the "state of the art" methodology is presented in this chapter. Later in the chapter, the stochastic inversion principles will be discussed more in detail since it is the main subject of the present project.

1.1 WEB–AVO INVERSION

Wave-equation based AVO (WEB-AVO) inversion [Gisolf and Van den Berg, 2012] solves the full elastic wave equation iteratively. One consequence of this approach is that multiple scattering and mode conversions are accounted for over a target interval.

The key points of the method are the following [Gisolf et al., 2017]:

- Surface recorded data is preconditioned by redatuming or migration. It makes the data more directly related to the target interval.
- A low-frequency background model constructed from well data is used as the starting model for the inversion.
- The wave equation is solved iteratively. Every iteration yields a more accurate approximation of the solutions for the wave-field and the properties.
- The isotropic elastic wave equation is defined in terms of the mass density and two elastic properties; therefore, the inversion solves directly for the following parameters: compressibility (inverse of bulk modulus), shear compliance (inverse of shear modulus) and density.

In the standard AVO inversion approach, the response of the earth is characterized by the reflection coefficients, which in turn can be converted to elastic properties. This approach comes from linearizing the earth's response. Mathematically, the reflection coefficients used in standard AVO inversion are linearisations of the Zoeppritz coefficients [Sheriff, 2002] [Gisolf, 2016] .

On the other hand, if one looks at the unlinearised full elastic wave equation, it is defined in terms of properties directly.

In the framework of reservoir geophysics, a thorough analysis [Gisolf, 2016] [Gisolf et al., 2017] for compressibility and shear compliance shows that these two properties are more directly related to hydrocarbon saturation and porosity changes than the impedances that are obtained from conventional AVO inversion. In addition, if one were to calculate compressibility and shear compliance from impedances, an accurate estimate of the density would be necessary .

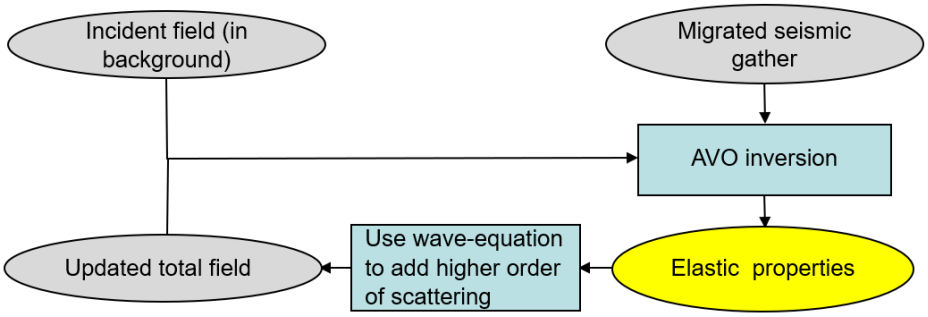

Figure 1.1: Deterministic WEB-AVO inversion workflow.

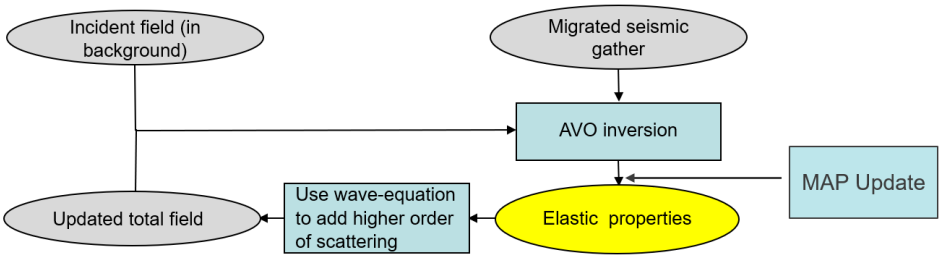

Figure 1.2: Stochastic WEB-AVO inversion workflow.

A simplified workflow for WEB-AVO inversion is summarized in figure1.1. In the first iteration the incident field in the background model is taken as a first approximation of the total wave-field and a kernel can be calculated for a linear data model that links the pre-conditioned seismic gather to the elastic properties to invert for. This kernel is used to compute a first estimate of the properties.

With this estimate of the properties, first order scattering in the wave-field can be calculated, which can be added to the incident field. With this improved estimate of the total wave-field a new inversion kernel is calculated, yielding an improved inversion estimate for the properties.

The essentially non-linear problem is solved iteratively, whereby in every iteration a higher order of multiple scattering is accounted for. To stop the inversion matching noise in the data, the AVO inversion in every iteration needs regularisation. The current development of the WEB-AVO inversion incorporates a sparse gradient regularisation based on a 'Cauchy' norm.

In the present work, an additional step will be included in the workflow. After the seismic gather has been inverted for the elastic properties, a maximum a posteriori estimation (MAP) update is performed as in figure 1.2. With the help of Bayes' Rule such update will incorporate a priori geological information.

The theory behind this stochastic approach will be further explained in the following section

1.2 STOCHASTIC INVERSION

From a statistical point of view, when we perform the inversion of observed data to derive model parameters, the results are not limited to a unique set of predicted parameters. A better representation of the results is a probability density function (PDF) over the model space [Buland and Omre, 2003].

As a natural consequence, an additional aim of inversion is to characterize the uncertainty of the results, and not only to find the best set of model parameters that fit the data.

In this context, a Bayesian framework is a natural choice for many geophysical inverse problems. In this kind of settings, the combination of prior knowledge with the information extracted from the measured data is possible [Scales and Tenorio, 2001].

1.2.1 Bayes' theorem

In the XVIII century, the British cleric Thomas Bayes formulated the theorem named after him[Bayes, 1763]. It relates the "direct" probability of a hypothesis conditional on a given body of data, to the "inverse" probability of the data conditional on the hypothesis [Joyce, 2019]. To better understand the theorem, we define as $P(E)$ the probability of having data E and we define $P(H)$, the probability that hypothesis H happens.

The direct probability of a hypothesis conditional on a given body of data means the probability of event H happening, conditional on the existence of data E. We note: $P(H|E)$.

The inverse probability of the data conditional on the hypothesis means the probability of having the body of data E conditional on the event H. We note: $P(E|H)$.

Bayes' theorem is then stated as:

$$P(H|E) = \frac{P(E|H) \cdot P(H)}{P(E)} \tag{1.1}$$

For the purposes of geophysical inversion, Bayes' theorem gets slightly modified by using probability density functions instead of single probabilities. The modified theorem states [Fichtner, 2019]:

$$\rho(\mathbf{m}|\mathbf{d}) = \frac{\rho(\mathbf{d}|\mathbf{m})\rho(\mathbf{m})}{\rho(\mathbf{d})} \tag{1.2}$$

Where:

- $\rho(\mathbf{m}|\mathbf{d})$ is the Posterior probability density function of the model $\mathbf{m}$ given the data set $\mathbf{d}$.
- $\rho(\mathbf{d}|\mathbf{m})$ is the Likelihood function.
- $\rho(\mathbf{m})$ is the Prior probability density function in the model space.

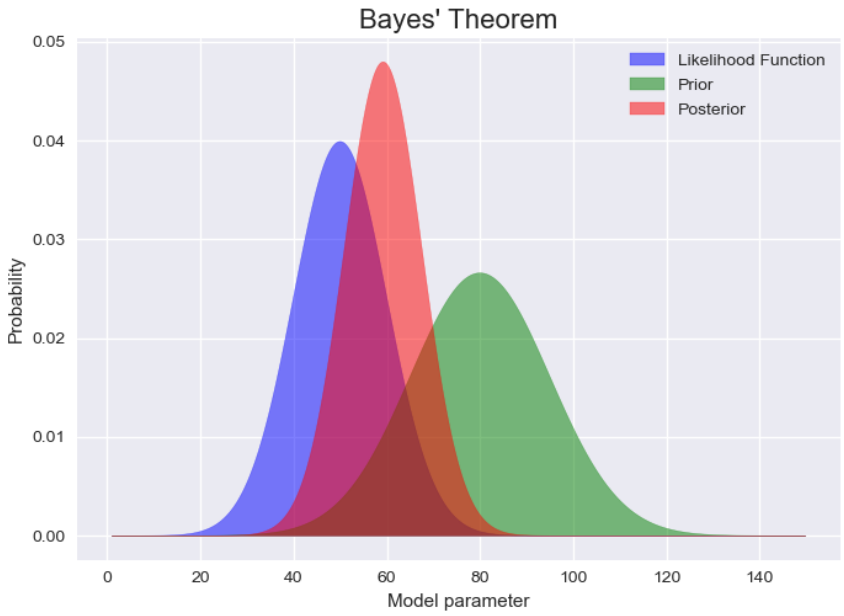

Figure 1.3: Schematic representation of Bayes' theorem using Gaussian functions as probability density functions.

- $\rho(\mathbf{d})$ is named the evidence or probability density function of the data, which acts as a scaling factor for the posterior. It is defined as:

$$\rho(\mathbf{d}) = \int_M \rho(\mathbf{d}|\mathbf{m})\rho(\mathbf{m})d\mathbf{m} \tag{1.3}$$

Figure 1.3 shows a simplified graph that depicts visually the theorem stated above. Two data sets of information are combined in the form of probability density functions. The blue curve, the likelihood function, is represented as a Gaussian function with a certain mean and standard deviation.

On the other hand, the green curve represents the Prior probability density function. It is represented by another gaussian curve but, as it will be explained later, the Prior probability function used in the present work is a complex non-gaussian multidimensional function.

Following Bayes' theorem, the posterior probability density function is obtained by multiplying the two previous functions and scaling the resulting function by the probability density function of the data. The resulting curve is the red curve.

The blue curve, the Posterior probability density function, is the solution of the stochastic/probabilistic inverse problem [Fichtner, 2019]. The function itself contains all the information we can possibly obtain by combining the prior information on the data (geological data obtained from well locations), the forward modelling theory (WEB-AVO inversion theory), and the model parameters.

1.2.2 Maximum a Posteriori Estimate

To find an estimate of the model parameters, a model that maximises the posterior probability density must be found. In the example presented above, the task is trivial since the Maximum a posteriori estimate is the mean of a Gaussian function.

The prior probability density distribution, in the present work, is a complex multivariate function. Consequently, conjugate gradients methods (or any other optimization method) can and are used to optimize the posterior and find the MAP estimate.

For the purpose of this research, we optimize the Posterior probability density function with an L-BFGS algorithm implementation [Liu and Nocedal, 1989].

For completeness the MAP Estimate [Fichtner, 2019] can be defined as:

$$\mathbf{m}_{max} = arg\ max\ \rho(\mathbf{m}|\mathbf{d}) \tag{1.4}$$

1.3 PRIOR PROBABILITY DENSITY FUNCTION

One of the simplest models of the subsurface is a layered model of the earth. Citing one of the fundamental principles of geology, Walther's law, "The various deposits of the same facies-area and similarly the sum of the rocks of different facies-areas are formed beside each other in space, though in a cross section we see them lying on top of each other" [Walther, 1894].

Every same or similar-facies layer is considered as a litho-stratigraphic unit that extends laterally. Layers can also be considered as a stratigraphic unit corresponding to a certain interval of geologic time.

For reservoir geophysical purposes, and for the purpose of the present work, the individual units are characterized by their thickness and property values (shear compliance M, compressibility κ, density ρ) [Sharma, 2019]

In exploration geophysics, the only accurate way to assess the real rocks in the deep underground is by drilling a well and correlate the stratigraphic units with the obtained seismic section/cube. The interpreter relies on the previous stated Walther's law and the principle of lateral continuity: "All rock layers are laterally continuous and may be broken up or displaced by later events".

The more wells are drilled, the more information about the spatial distribution of the stratigraphic units is available.

Why to incorporate this prior geological knowledge into the inversion algorithm? The WEB-AVO inversion is a non-linear method that, although unlikely to get stuck in local minima, may not converge [Gisolf et al., 2017]. Incorporating prior geological information from well locations can improve the overall result by pulling the model properties towards a real geological model.

How does one define the prior probability density function? In the simple classical stratigraphic model, we consider that all the elements of a stratigraphic unit have the same absolute property value. This is not true; a stratigraphic unit can have property value variations within itself, even anomalous but thin sublayers that are too small to make a stratigraphic unit themselves. To honour the natural heterogeneity of a geological formation, we can define every property value as a random variable with a Gaussian distribution, i.e., a distribution with a mean value and a certain spread characterized by a standard deviation.

In addition to this, the thickness of the layer can also be treated as a random variable with a Gaussian distribution. In practice, the thickness of a layer can dif-

fer significantly from one location to another. In some cases, one can define the boundary of two units as a transition zone rather than a fixed set boundary.

All Gaussian distributions characterizing a unit extend from minus infinity to plus infinity. The part of the Gaussian on the negative interval means physically that the layer doesn't exist. For property distributions usually the part under the Gauss curve over the negative property axis is negligible. However, for Gaussian layer thickness distributions, a significant part of the curve may extend over negative thicknesses. The integral over the negative interval is then replaced by proportional Dirac delta-function at '0' thickness, representing the probability that that layer is absent.

Third and last, another degree of freedom can be added by allowing ramps instead of constant property values over a layer. Geologically, coarsening or fining upward trends can create increasing or decreasing property values within one unit. To honour this type of geology, different property values are set at the top and bottom of the unit.

Therefore, the prior probability density distribution that characterizes a layer is a function of random variables with Gaussian distributions for the three property values and a truncated Gaussian distribution for the thickness of the layer.

1.3.1 Layer-based model vs Grid-based model

The Prior model described above is designed based on the concept of layers. However, the WEB-AVO inversion is defined on a grid-based model, i.e. the data is inverted for the properties of individual grid points over the target interval.

Consequently, the layer-based prior model has to be transformed to a grid-based model using a Gaussian mixture model. It describes the multi-modality of the distribution as the weighted sum of individual Gaussian distributions [Sharma, 2019]:

$$P_P(\mathbf{m}) \propto \prod_{i=1}^{Nz} \sum_{j=1}^{NL} \sum_{k} w_{ijk} N(\kappa_i, M_i, \rho_i, \mu_{jk}^{(\kappa)}, \mu_{jk}^{(M)}, \mu_{jk}^{(\rho)}, \sigma_j^{(\kappa)}, \sigma_j^{(M)}, \sigma_j^{(\rho)}) \tag{1.5}$$

Where Nz is the number of grid-points, NL is the number of layers, N is a normal (Gaussian) distribution for the grid-point i with properties κ_i, M_i and ρ_i; with mean values μ_{jk}^{κ}, μ_{jk}^{M} and μ_{jk}^{ρ}; and with standard deviation σ_j^{κ}, σ_j^{M} and σ_j^{ρ}. The i index refers to the grid-point, j refers to the layer and k refers to the position inside the layer since ramps can be handled. The vector $\mathbf{m}$ contains all grid-based properties κ , M and ρ. All grid-points are considered statistically independent, which is consistent with the definition of the layer-based model where the property of a layer is supposed to be a random process over the extent of the layer

The tensor $\mathbf{W}_{ijk}$, which will be called the 'weight matrix', represents the probability that a specific grid-point i is sitting in the jth layer with a position k inside that layer. This matrix is uniquely determined by the layer thickness distributions and is the main feature that transforms our prior from a layer-based model to a grid-based model.

The weight matrix is a three dimensional tensor. For the purpose of visualisation, figure 1.4 shows a section of the tensor where the third dimension, the relative position inside the layer, has been summed away. The image shows the probability of every single grid-point i to be in layer j.

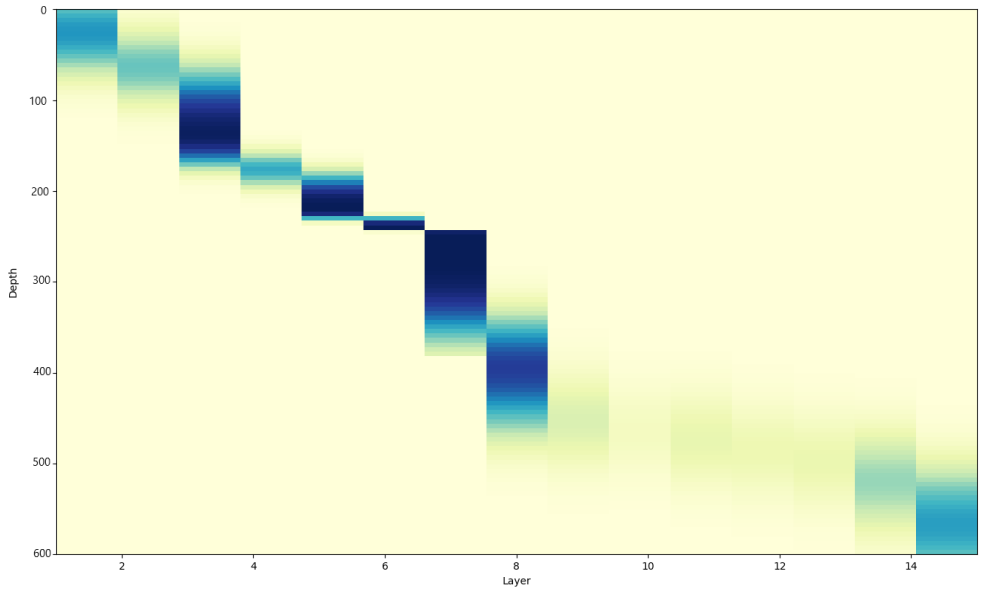

Figure 1.4: Weight matrix 2D representation. It depicts the probability of every grid point i to be sitting in the layer j.

One of the main tasks of the present project will be to build the prior function from well data.

1.4 LIKELIHOOD FUNCTION

In the WEB-AVO inversion, the model parameters vector $\mathbf{m}$ contains the values for κ, M and ρ for all different grid-points in the target interval.

The equation used in the box called AVO inversion in figure 1.1, is :

$$\mathbf{d} = \mathbf{K}\mathbf{m} \tag{1.6}$$

Where $\mathbf{d}$ is the observed data to be inverted, and $\mathbf{K}$ is the kernel used during that particular outer-loop iteration.

The solution of the above equation is the solution for the inverse problem. It will be referred as the maximum likelihood estimator and will be noted $\mathbf{m}_{mle}$.

The Likelihood function can be understood to be a Gaussian noise distribution. This is the distribution of the noise in the data that explains why the data can be different from the predicted data when the model used for the prediction is supposed to be the truth. A proper equation for the likelihood function is:

$$P_L(\mathbf{d}|\mathbf{m}) \propto \exp^{-\frac{1}{2}|\mathbf{d}-\mathbf{d}(\mathbf{m})|^2/\sigma_N^2} \tag{1.7}$$

Where $\mathbf{d}$ is the data to be inverted, $\mathbf{d}(\mathbf{m})$ is the notation for the data being modelled given a model vector $\mathbf{m}$ and σ_N^2 is the variance of the Gaussian noise present in the data.

One can develop further the expressions for $\mathbf{d}$ and $\mathbf{d}(\mathbf{m})$:

$$\mathbf{d} = \mathbf{K}\mathbf{m}_{mle} + \mathbf{r} \tag{1.8}$$

$$\mathbf{d}(\mathbf{m}) = \mathbf{K}\mathbf{m} \tag{1.9}$$

The first expression explains that the inverted data is the data estimated with $\mathbf{m}_{mle}$ plus the unexplained part of the data, the residual $\mathbf{r}$. For real data it is safe to assume that r is much smaller than the noise in the data, i.e. the inversion has matched most of the noise in the data. To stay on the safe side for the analysis of the uncertainty of the prediction, we will assume that r does not contain a significant part of the real noise in the data and, therefore, does not have to be taken into account.

If the expressions above are inserted into the equation for the likelihood function, the result is:

$$P_L(\mathbf{d}|\mathbf{m}) \propto \exp^{-\frac{1}{2}(\mathbf{m}-\mathbf{m}_{mle})^T \mathbf{C}_m^{-1}(\mathbf{m}-\mathbf{m}_{mle})} \tag{1.10}$$

Where $\mathbf{C}_m^{-1} = \frac{\mathbf{K}^T\mathbf{K}}{\sigma_N^2}$ is the data covariance matrix in the model space.

1.4.1 Estimate of the noise in the data

One key parameter that needs to be understood is the estimation of the variance of the noise in the data. If the estimation of the noise in the data is a small number, our likelihood function will be a very narrow Gaussian function. Consequently, it won't allow the prior function to incorporate new information. In a sense, one is then overconfident and too positive about the accuracy of the inversion results.

This number plays a major role in the stochastic inversion. It can also be used to weight the seismic information relative to the prior information obtained from the wells and vice versa. If the information obtained from the seismic inversion is to be trusted more, then a small number must be set for the estimate of the noise variance. On the other hand, if the prior is to be trusted over the seismic information, then a bigger estimate of the noise must be given.

In the present project, we propose as an accurate estimate of the noise in the data, the residual coming from the seismic-to-well tie at the well location. If the residual is close to zero, it means that the well data can explain perfectly the seismic information, in which case there is little to no noise in the seismic data. On the other hand, if the residual of the seismic-to-well match is large, it means that even using the best estimate of the truth, which is the information obtained from the well, there is some noise that may be matched by the inversion, leading to incorrect predictions. This is indeed the case for real data.

One of the tasks of the present project will be to obtain and test an optimal value of the estimate of the noise from a seismic-to-well tie procedure at a well location.

1.4.2 Estimate of the uncertainty of the method (WEB-AVO inversion)

There exists another source of uncertainty that needs to be assessed and incorporated in the uncertainty assessment: the non-uniqueness of the inversion method.

Even when using optimal methods to regularize the inversion, it may be that the inversion doesn't perform well for specific grid-points. It will give a false feeling of certainty about the obtained property values.

To assess the uncertainty of the method we propose the use of random starting models derived from the Prior distribution. As explained in the previous section, the Prior function is built from the interpretation of well data and takes the form of a mixture of Gaussians.

By taking random realisations from the Prior and using them as starting models for the inversion, Gaussian distributions for every single grid-point over the target interval are expected. Optimally, one may expect to find very narrow Gaussian distributions, meaning that even the wildest and less likely random realisation will give optimal results.

The assessment performed in the present project will show that this is not the case. The Gaussians for every grid point can be interpreted as the uncertainty of the inversion method. Variances and covariances can be computed for every grid point and the results can be added to the covariance matrix of the posterior.

1.5 POSTERIOR PROBABILITY DENSITY FUNCTION

To obtain the posterior probability density function, Bayes' theorem bust be recalled. By using the notation implemented in the previous sections one has:

$$P_{Po}(\mathbf{m}|\mathbf{d}) \propto P_L(\mathbf{d}|\mathbf{m})P_P(\mathbf{m}) \tag{1.11}$$

If the expressions for P_L and P_P are inserted, one has:

$$\begin{aligned} P_{Po}(\mathbf{m}|\mathbf{d}) \propto & e^{-\frac{1}{2}(\mathbf{m}-\mathbf{m}_{mle})^T \mathbf{C}_m^{-1}(\mathbf{m}-\mathbf{m}_{mle})} \times \\ & \prod_{i=1}^{Nz} \sum_{j=1}^{NL} \sum_{k} w_{ijk} N(\kappa_i, M_i, \rho_i, \mu_{jk}^{(\kappa)}, \mu_{jk}^{(M)}, \mu_{jk}^{(\rho)}, \sigma_j^{(\kappa)}, \sigma_j^{(M)}, \sigma_j^{(\rho)}) \end{aligned} \tag{1.12}$$

The function P_{Po} needs to be maximized to find the maximum a posteriori estimate. Taking another approach, an objective function F_{Post} can be built by taking the negative logarithm of the posterior distribution, in which case, the function needs to be minimized.

$$F_{Post}(\mathbf{m}) = \tfrac{1}{2}(\mathbf{m}-\mathbf{m}_{mle})^T \mathbf{C}_m^{-1}(\mathbf{m}-\mathbf{m}_{mle}) - \sum_{i=1}^{Nz} \ln \sum_{j=1}^{N_L} \sum_{k} w_{ijk} N_{i,j,k} \tag{1.13}$$

where $N_{i,j,k}$ is short-hand for the N function in the previous equation.

1.5.1 Minimization of the objective function

For the purpose of this research, the optimization of the objective function will be done with an L-BFGS algorithm implementation [Liu and Nocedal, 1989].

2 CHAPTER 2: METHODOLOGY

The present work has some clear objectives that need to be recalled:

- Estimate the noise in the data .
- Analyse effect of using prior information on the deterministic WEB-AVO results.
- Estimate uncertainty of the inversion with the help of ensembles of starting models.

To attain the objectives, a clear methodology had to be followed. Some of the methods are standard procedures widely used in explorations geophysics, some others are specifically designed for the present project.

1. Well interpretation: prior model creation.
2. Seismic-to-well tie: wavelet extraction and data noise estimation.
3. Deterministic inversion: parameter tuning and choice of target interval.
4. Random realisations: method uncertainty estimation.
5. Stochastic Inversion: single location and 2D section.
6. Uncertainty assessment.

2.1 WELL INTERPRETATION: PRIOR MODEL CREATION

In exploration, well logs are traditionally used to correlate geological units and assist in the identification of structures [Asquith and Krygowski, 2004]. Petrophysicists make use of well logs for characterizing the physical properties of the rocks in the subsurface. Properties like lithology, porosity, pore geometry and permeability can be derived from the physical properties measured down-hole. Geologists can also interpret boundaries, depths and thicknesses between the different lithological units.

In order to build the prior probability density function , we need to create a geological layered model. Every layer is characterized by its thickness, compressibility modulus κ, shear compliance M (inverse of shear modulus μ) and density ρ. The elastic parameters are computed from V_P, V_S and ρ log values using the following relationships:

$$\kappa = \frac{1}{\rho(V_P^2 - \frac{4}{3}V_S^2)} \tag{2.1}$$

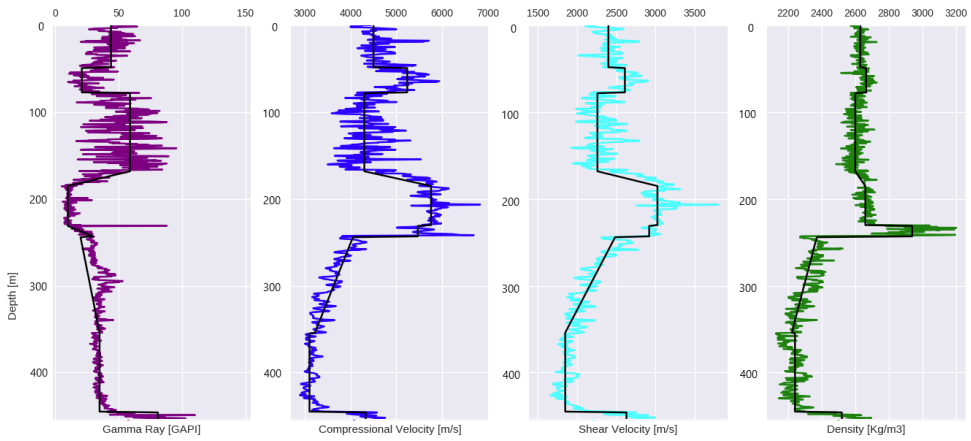

Figure 2.1: Well interpretation example on creating a blocky layered model from Gamma ray, compressional velocity, shear velocity and density logs.

$$M = \frac{1}{\mu} = \frac{1}{\rho V_S^2} \tag{2.2}$$

Any other log like gamma ray, acoustic impedance, porosity, water saturation, can be used to define the stratigraphic units for which prior distributions have to be derived.

Figure 2.1 shows an example of an interpretation performed on a specific interval using Gamma ray, compressional velocity, shear velocity and density logs.

First, boundaries for all the layers in the target interval must clearly be defined in depth. By choosing a top layer depth and a bottom layer depth, the thickness of the layer can be determined. The interpreter assigns a value for the standard deviation around the absolute value of the thickness. A layer with a mean thickness and a standard deviation will be treated as a Gaussian distribution.

A thin layer with a high standard deviation may have part of its distribution curve on the negative thickness axis. Physically, negative thickness is an impossible concept, but the area under the curve on the negative side is replaced by a Delta function at zero meters. It is the probability that that layer doesn't exist. Figure 2.2 is an illustration of this scenario. Graph (a) shows the original Gaussian distribution and graph (b) shows the same distribution with a Delta function replacing the curve on the negative side of the thicknesses.

For every layer property, the mean consists of a mean at the top of the layer and a mean at the bottom of the layer. By flexibly choosing a top unit value and a bottom unit value, property ramps inside the layer can be handled. Variances and covariances can later be computed from the logs.

In figure 2.1 a unit starting around 250 meters seems to be a coarsening upward sequence that decreases its velocity values for about 100 meters. It is represented by a ramp.

The prior probability density function is a very versatile tool that can be used in many ways:

- It is the prior probability density function that will help compute the posterior.
- The prior function is a mixture of Gaussians, it can be used to compute the mean of the mixture in the grid-based domain. This so called "grid-based

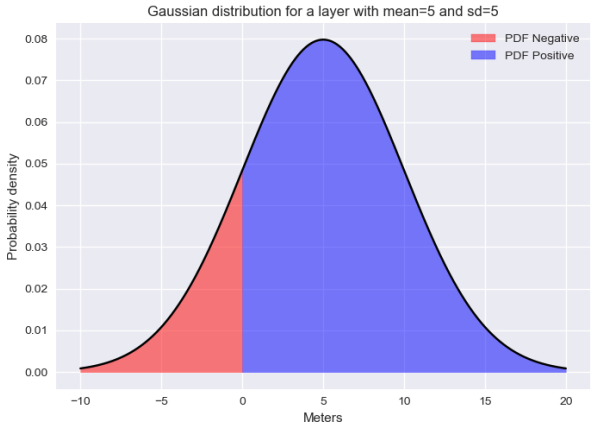

(a) Gaussian distribution for a layer with negative thickness.

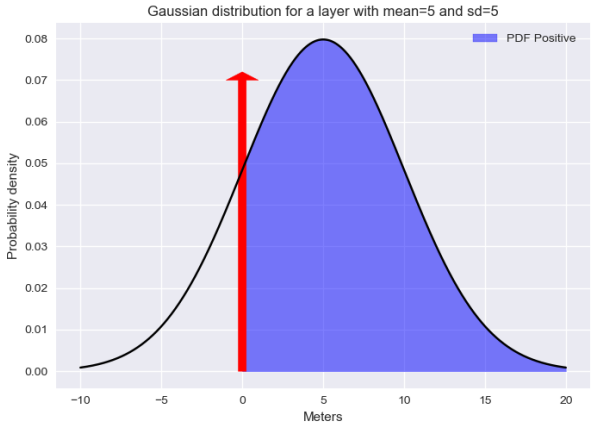

(b) The negative part of the PDF is replaced by a Delta function proportional to the area under the Gaussian curve at o. Physically it is the probability that the layer doesn't exist.

Figure 2.2: Gaussian distribution for a layer with negative thickness.

mean" can be used as a starting model since it is the best unbiased estimate of the truth.

- A severely smooth version of the grid-based mean can be used as a background model for the WEB-AVO inversion.

2.2 SEISMIC-TO-WELL TIE: WAVELET EXTRACTION AND DATA NOISE ESTIMATION

Any seismic inversion approach requires the extraction of a characteristic wavelet inside the target interval. The present work has a second interest in doing the wavelet extraction: the residual of the seismic-to-well tie will be used as an estimate of the noise in the data.

The seismic-to-well tie is performed in one of the toolboxes of Helios. Before, conversion of the seismic image gather from the offset domain to the ray-parameter (horizontal slowness) domain is required.

One problem encountered when trying to match well-log and seismic data is the different resolution they provide. Modern technology allows logging tools to sample as finely as several centimetres. On the other hand, seismic data loses resolution as it goes deeper in the underground.

The reflection of seismic waves doesn't arise from a single point but from an area called the Fresnel Zone [Liner, 2016]. After migration the relevant measure for horizontal resolution is the Rayleigh radius [Gisolf and Verschuur, 2010]. This measure is the limit of the lateral resolution of seismic data. In other words, two different objects close to each other that find themselves inside the Rayleigh radius zone cannot be individually distinguished. The Rayleigh radius is a function of the average velocity, dominant frequency and depth.

To better match the seismic data and obtain a wavelet characteristic enough of the areas around the well, the logs must be smoothed. Ideally this should be a lateral smoothing that bridges the gap between the width of the borehole and the seismic Rayleigh radius. Since lateral smoothing of well-logs is not possible, we rely on Walther's law again to simulate this lateral smoothing of the logs by a vertical smoothing.

For full elastic wave-equation based modelling of well synthetics we could use the forward modelling engine of the WEB-AVO inversion, but for well synthetics it is more convenient to use the Kennett's method[Kennett, 1979], which is also an exact method in the sense that it solves the wave-equation for every thin layer and connects all these solution by boundary conditions. In addition, for synthetic inversion experiments it is important to avoid the so called inverse crime, by which is meant that the inversion uses exactly the same modelling by which the data was generated.

The seismic-to-well tie tries to match the synthetic data obtained from Kennett modelling, with the observed seismic data. The better the match, the smaller the residual will be. High values for the residual mean that the seismic data is polluted with noise.

The present work will treat the residual of the seismic-to-well match as the best estimate we have of the noise in the data.

Such estimate will be used to compute the likelihood function as discussed in the previous chapter.

2.3 DETERMINISTIC INVERSION: PARAMETER TUNING AND CHOICE OF THE TARGET INTERVAL

2.3.1 Background Model

Once the wavelet has been extracted, a background needs to be computed, which is required by WEB-AVO inversion. It is important that there is no overlap between the temporal bandwidth of the background function and the bandwidth of the data, this is a requirement since the WEB-AVO inversion uses the Wentzel-Kramers-Brillouin-Jeffreys(WKBJ) approximation to compute the incident field [Gisolf and Verschuur, 2010].

The background is a severely smoothed version of the true logs. In between wells the backgrounds are interpolated between the backgrounds extracted at the well locations. As discussed before, a severely smoothed version of the grid-based mean can also be used as background.

2.3.2 Parameter tuning

The WEB-AVO inversion is dependent on different pre-processing on the data and different parameters proper for the inversion.

Choices must be made on the amount of regularization controlled mainly by two parameters:

- Conjugate Gradient steps: the inversion carried out in the box labelled AVO inversion in figure 1.1 relies on a conjugate gradient method to find a solution to the inverse problem. The optimal number of CG steps must be tested. A too high number of CG steps could lead to overfitting the noise in data.
- Sparse gradient weight: This parameter controls the blockiness of the inversion result. A too high number could lead to loss of resolution.

Other parameters that need to be tuned are the desired amount of field updates (Outer loop iterations) and damping on rho when one decides to invert for all three parameters: κ, M and ρ.

2.3.3 Target interval

WEB-AVO inversion accounts for all the mode conversions and multiples inside a target interval. For research purposes, target depth intervals of around 1000 meters will be investigated. One important characteristic to keep in mind is the starting point of the interval. Experience from Delft Inversion has shown that a starting point far away from major events leads to better results.

2.4 RANDOM REALISATIONS: METHOD UNCERTAINTY ESTIMATION

A mixture of Gaussian functions has been created as a prior probability density function. Random realisations for every single point in the target interval are drawn from the prior distribution and they are used as the starting point for the WEB-AVO deterministic inversion.

A minimum of 30 to 50 random realisations are enough to create histograms on the inversion results for ever grid-point. Meaningful statistical data such as the variance and the covariance are then extracted.

In the present work, this uncertainty estimation is treated as the uncertainty due to the inversion method. These covariances are added to the covariances derived from the posterior, around the MAP location.

2.5 STOCHASTIC INVERSION: SINGLE LOCATION AND 2D SECTION

The inversion of seismic data is tested and tuned at the well location to obtain optimal results. The results of the inversion are compared to the smoothed version of the log properties, as a benchmark.

Once optimal inversion results are obtained, the inversion can be carried out at all locations. In the present work and for research purposes a 2D challenging section has been selected to test the stochastic WEB-AVO inversion.

The 2D section has been selected as an arbitrary line between three wells. Prior geological information is extracted from the three wells and correlated to create three prior probability density functions at the three well locations.

For the inversion of the 2D section other practicalities need to be taken care of:

- Interpolation of the prior: the prior is defined at the three well locations, but the thicknesses and value properties need to be interpolated for every location.
- Background (Low-frequency) model: The background at well location is a very low frequency model of the property logs. As part of this project a background model for the 2D section is created by interpolating and filtering the grid-based mean of the prior between the three well locations. The interpolation is carried out before the filtering to ensure the background for every location has the same wave-number content.
- Starting model: The grid-based mean from the prior is the best estimate we have about the truth. Therefore, it can be used as a starting model to constrain and possibly improve the deterministic inversion results. Once the prior model has been established everywhere along the 2D line, a local grid-based mean can be created to compute the background model and to be used as a starting model for every location.

3 CHAPTER 3: CASE STUDY

In this chapter a quick overview of the geological setting and challenges of the case study will be given. The processing and interpretation of the data before the inversion will be presented.

3.1 PRESENTATION OF THE STUDY CASE

The study case is a real data setting provided by Shell. The study area is covered by a full azimuth seismic survey with offsets ranging from 1200 to 6000 meters.

Inline and crossline separation are 20 m and 12.5 m respectively and the recorded time goes up to 9000 ms.

The surveyed area is inside a passive margin region with salt complexities at the basement.

For the purpose of testing the stochastic WEB-AVO inversion three representative wells of the area were carefully selected. An arbitrary line was drawn between well 1 and well 2 and between well 2 and well 3. One of the main objectives of the present project is to test the stochastic inversion by inverting the seismic data along the 2D line. Figure 3.1 shows the relative location of the wells and the drawn 2D line that will be used in the current project. A fault intercepts the section between well 1 and well 2.

The overall complexity of the area is the definition of the base of a reservoir located around 1000 m depth. Major horizons are well defined in the wells and recognized on seismic. The overburden formation, hard carbonates, laying on top of the reservoir is characterized by a high velocity and very anomalous high density. It creates a strong velocity contrast that allows an easily definition of the top of the reservoir.

The reservoir is found inside an aeolian sedimentary system with fluvial packages either laying below the aeolian formation or interbedding in it. The aeolian/fluvial sands transition to salt at the bottom of the basin.

Small acoustic contrast at reservoir level, inside the aeolian sand formation and at the transition from aeolian/fluvial sands to salt make the definition of the base of the reservoir a challenging and difficult task.

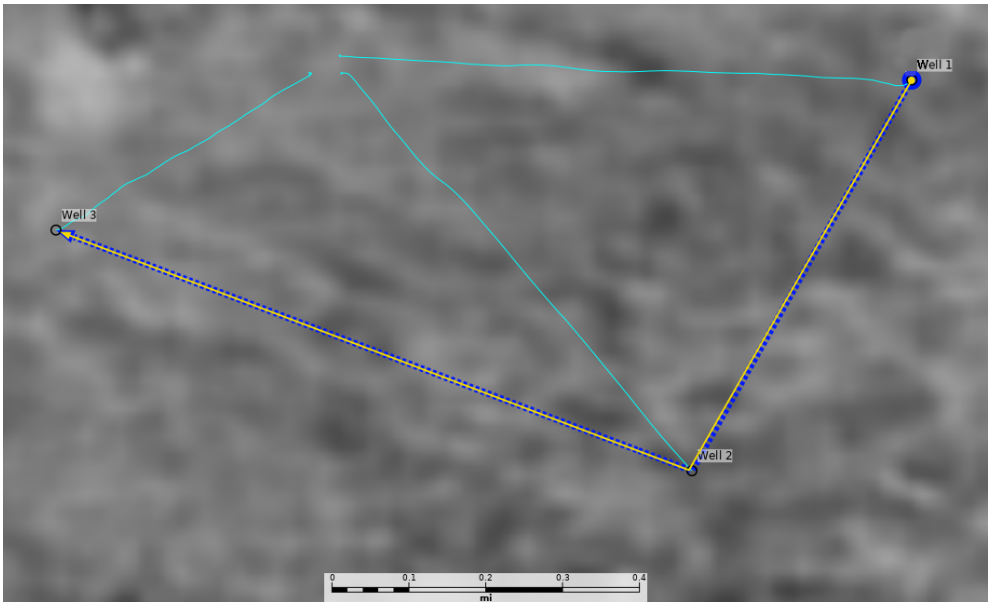

Figure 3.1: Relative location of wells 1, 2 and 3. These wells were carefully selected to test stochastic WEB-AVO inversion on a section crossing all three wells. The wells are deviated, and the cyan lines represent a surface projection of the trajectory of the wells.

3.2 PRIOR BUILDING: WELL INTERPRETATION

The three wells used in the present project were selected because of their geological interest. Only one of them has more or less continuous log coverage. Well 2, found in the middle of the 2D section was logged down to reservoir level and stopped before the salt formation. Well 1, found on one of the extremes of the section was very poorly logged and contains incomplete data all along the overburden and at reservoir level. Well 3, found on the other extreme of the section was logged but stopped before the reservoir level. Velocity logs seems to be incomplete at the bottom of the overburden.

The challenge in building the prior is to make a careful interpretation of the three wells to further correlate the different formations along the 2D section. Missing information must be inferred from one well to another by correlating property values and unit thicknesses.

Figures 3.2, 3.3 and 3.4 show the interpretation made respectively on wells 1, 2 and 3, the true logs are coloured in blue, turquoise and green and the unit interpretation is coloured black. The tops of the wells, gamma ray, acoustic impedance, compressional velocity, shear velocity and density logs have been used to define the main stratigraphic units.

Top and bottom unit values can be chosen independently. In this manner, increasing or decreasing values can be grouped and managed into a single unit.

3.2.1 Well 2 Interpretation

To begin with, an interpretaton of well 2 will be described in detail since it is more complete than the other two. Interpretation of well 1 and 3 will be discussed later.

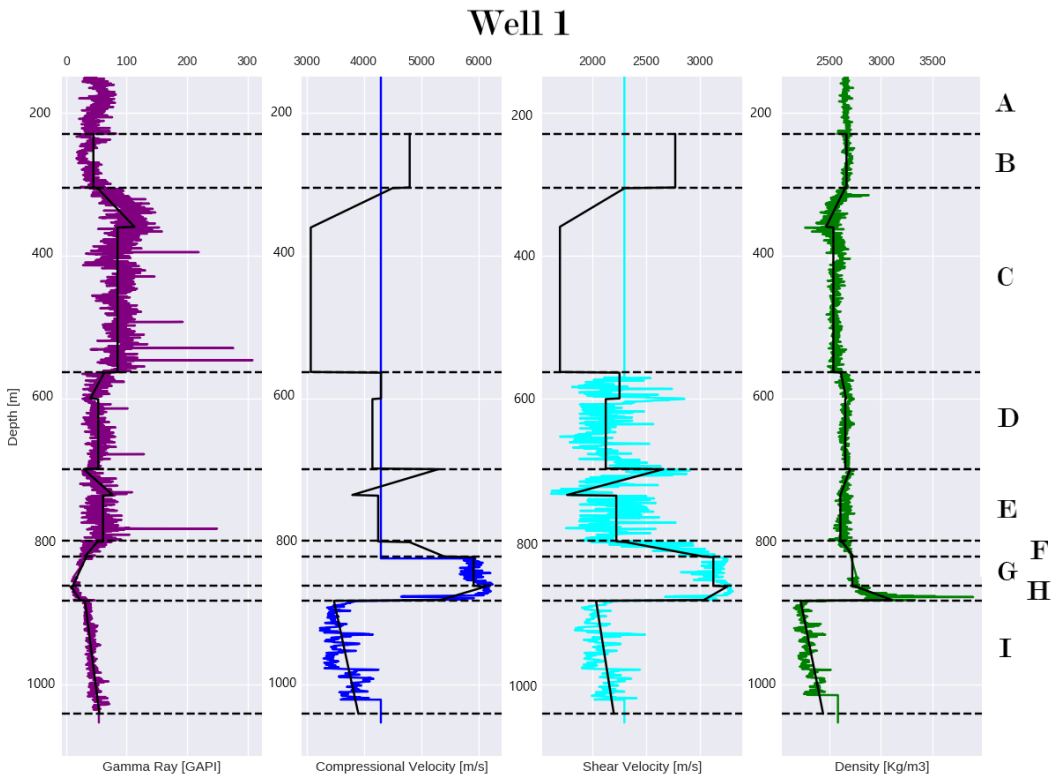

Figure 3.2: Well 1 displaying target interval where units have been interpreted inside every formation.

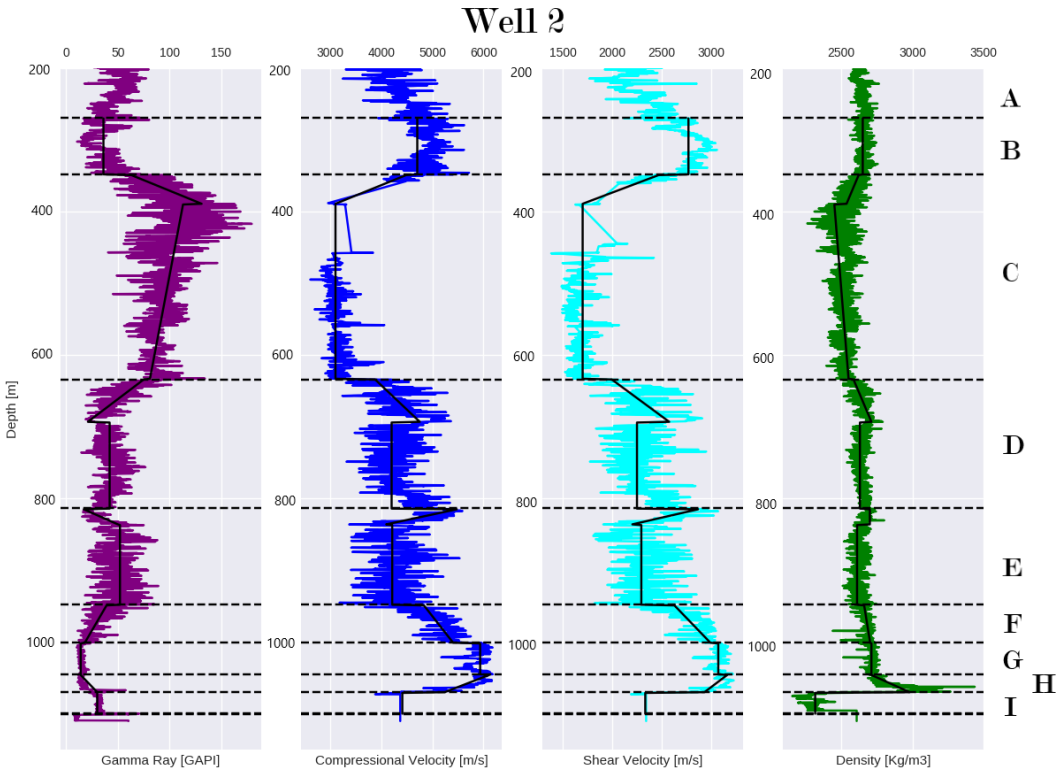

Figure 3.3: Well 2 displaying target interval where units have been interpreted inside every formation.

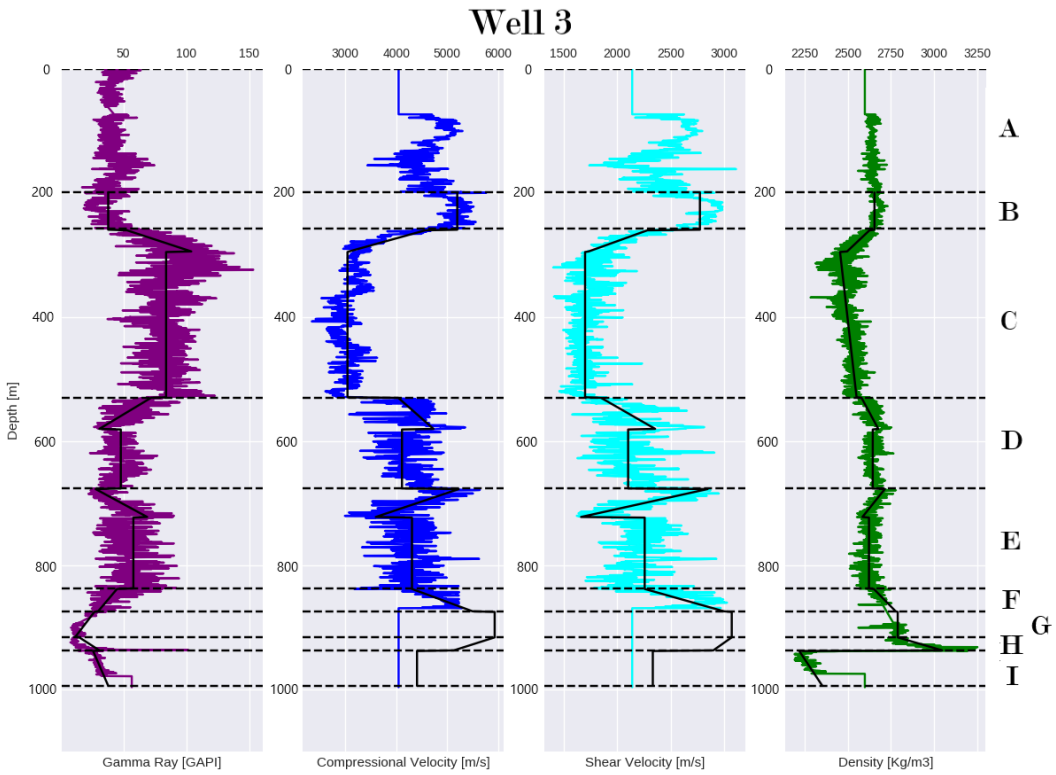

Figure 3.4: Well 3 displaying target interval where units have been interpreted inside every formation.

The interpretation of well 2 (figure 3.3) yields 13 lithostratigraphic units. It is used as a reference for the interpretation of the other two wells. When the word "formation" is used, it refers to the formations interpreted by the geologist and used in the naming of the well-tops. When the word "unit" is used, it refers to the lithostratigraphic unit interpreted by the author of this report to build the prior.

The first unit goes from 100 m to 348 m. This unit includes the first two overburden formations A and B before the first major velocity contrast. As we mentioned before, it is advised to keep the start of the target interval away from big velocity contrast events. The second formation C has been divided into two units. One thin unit going from 348 m to 374 m and another one going from 374 m to 634 m. The first one captures the transition to softer and more porous materials, and the second one captures the thick formation C itself.

Formations D and E have been interpreted in a similar way. Both have been divided into two units. The first unit in both cases emulates a ramp going from low to high velocity materials in formation D and high to low velocity materials in formations E. The second unit in both cases has more constant property values. This column going from 634 m to 948 m has henceforth been divided into four units.

Formations F captures a rapid transition to more competent materials with high velocity values going from 948 m to 1001 m. Formation G has constant high velocity values and its top and bottom are located at 1001 m to 1045 m respectively. Each one of them have been interpreted as a single unit.

Formation H needs a deeper discussion. While the velocity values for this formation drop significantly over a short interval, density values increase and some readings show densities in the order of 3.1 to 3.3 kg/m^3. The anomalous formation has the peculiarity that it decreases its velocity the denser it becomes. Specialists

have discarded errors in the readings or instrumentation since all the wells around the area show the same behaviour for formation H. Even if the exact nature and lithology of the formation is still under discussion, the great velocity contrast makes a clear reflector that makes the top of the reservoir an easy target. It has been interpreted as one unit with different top and bottom property values going from 1045 m to 1070 m.

Formation I is the aeolian sand where the reservoir is located. Log information from other wells in the area, not presented in this report, has shown that the aeolian formation is followed either by beds and interbeds of shaley sands coming from fluvial environments, or by salt. It is estimated from other logs that the fluvial sands have a 40% probability of being present and an average thickness of 15 meters. Concerning the salt, it is assumed to be a very thick layer with standard salt properties.

Formation I can be expressed as one unit going from 1070 m to 1099 m according to the interpretation from the gamma ray and density logs, at this level. Velocity data is non-existent. Formation J, the fluvial sand, is not present in the logs, so its average property values have been derived from other wells in the area and the standard deviations of the properties are estimates because they cannot be computed from the log.

To derive the standard deviation for the thicknesses, we must compute the Gaussian for a layer having an average thickness of 15 meters and 40% chance of existing. Mathematically it means that we need to derive the mean and standard deviation of a Gaussian distribution that has the following two characteristics:

- The integral of the curve from -∞ to 0 is 0.6.
- The average value of the curve in the interval 0 to ∞ is 15 m.

Since a Gaussian distribution is symmetrical, we can also compute a Gaussian with the following characteristics and remember to change the sign of the mean.

- The integral of the curve from -∞ to 0 is 0.4.
- The mean value of the curve in the interval -∞ to 0 is -15 m.

If we assume that a spread of 3σ includes 99.7% of the area under the Gaussian curve, the equations to be solved are:

$$CDF(0, \mu, \sigma) = 0.4 \tag{3.1}$$

$$\frac{1}{0-(-3\sigma)}(CDF(0, \mu, \sigma) - CDF(-3\sigma, \mu, \sigma)) = PDF(-15, \mu, \sigma) \tag{3.2}$$

Where $CDF(\mu, \sigma)$ is the Cumulative Density Function and $PDF(\mu, \sigma)$ is the Probability Density function of a Gaussian distribution with meanμ and standard deviation σ. They are given by:

$$CDF(x, \mu, \sigma) = 0.5(1 + erf(\frac{x-\mu}{\sigma\sqrt{2}}) \tag{3.3}$$

$$PDF(x, \mu, \sigma) = \frac{1}{\sigma\sqrt{2\pi}} \exp^{-0.5(\frac{x-\mu}{\sigma})^2} \tag{3.4}$$

And $erf(z)$ is the Gaussian error function.

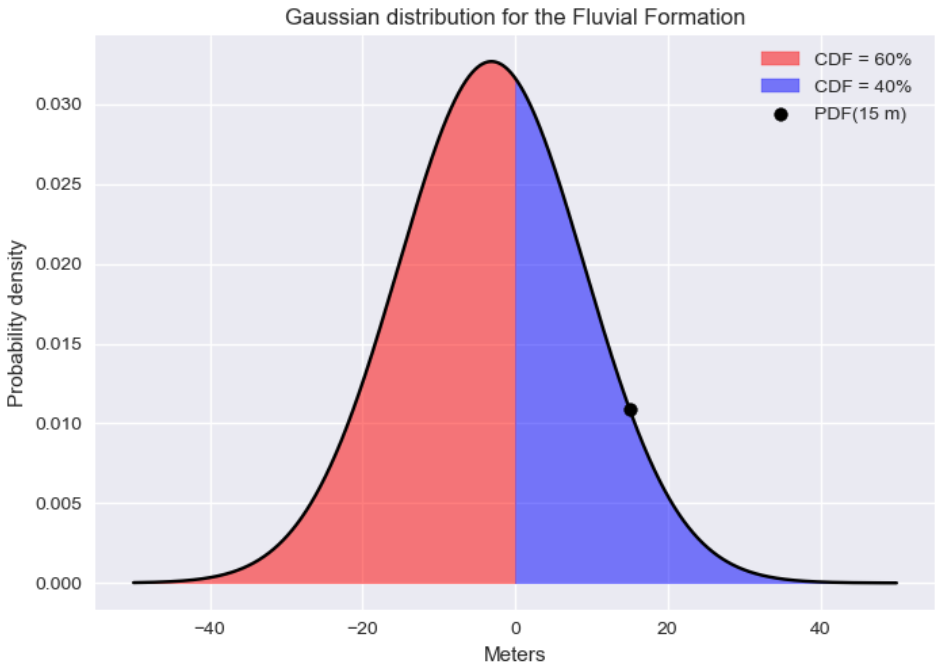

Figure 3.5: Gaussian distribution for the fluvial formation, the red area is 60% of the total curve integral, it is the probability that the layer is not existent. During the building of the prior the red area is replaced by a proportional delta function at x=0. The blue area represents the probability of the layer existing. The average value of the layer is 15 m.

Solving the system of equations described above we obtain: $-\mu$ = 3.0943 and σ=12.2137. Figure 3.5 shows the derived Gaussian distribution for the Fluvial unit.

Finally, the salt unit will be set as a very thick formation that can be extended in length. Standard values such as V_P= 4500 m/s, V_S= 2250 m/s and ρ= 2050 kg/m^3 will be used. Setting standard deviations of 2% of the absolute value of the properties is enough to create a Gaussian distribution that includes local variations of the properties of the salt.

3.2.2 Well 1 and 3 interpretation

Following the same methodology and reasoning used in the interpretation of well 2, well 1 and 3 have been interpreted. The target interval misses major velocity information in well 1. An interpretation for unit thicknesses and property values inside formations D, E, F, G, H and I has been performed. The thickness interpretation for the remaining units was carried out using the tops of the well and gamma ray and density logs. For the property values of the missing units, the interpreted means and variances from well 2 have been used. Although the aeolian reservoir formation was generously logged, the fluvial formation or the salt was never reached.

Well 3 contains information on formations A to F. The rest of the formations don't have velocity information. The same procedure was followed. Unit thickness interpretation has been carried out with the help of the tops of the well and gamma ray and density logs while the property means, and variances are borrowed from well 2.

Figures 3.6, 3.7 and 3.8, show the interpretation made on the three wells for compressional velocity, shear velocity, and density. Well 1 and 3 borrow the missing properties and patterns from the interpretation done on well 2.

3.3 SEISMIC-TO-WELL TIE

Seismic information at the location of well 2 was extracted to perform the seismic-to-well tie and to derive a wavelet. The migrated seismic image gather is converted to the ray-parameter domain by ray-tracing through a locally stratified overburden model. Kennett synthetics are used for the seismic-to-well tie and, once a wavelet has been extracted, to create synthetic data to test and benchmark the WEB-AVO inversion.

The best inversion results for synthetic data were obtained with the following conditions:

- Reconstruction of missing parts in the logs.
- 300 m salt extension .
- Filtered seismic data with a low-pass filter (5-10 Hz).

Even if well 2 is the most complete out of the three wells, it still has a 70 m interval around 7200 m depth where no information is available. In order to have a better seismic-to-well match, the velocity properties were reconstructed for the interval using Gardner's relationship. At the bottom of the well, velocities for the aeolian layer are predicted, a thin fluvial layer is set, and finally, salt properties are introduced.

Strong events at the bottom of the target interval are problematic to fit. To avoid creating instabilities due to the truncation of the log, salt properties are artificially added to the salt over a 300 m interval. The common consensus from specialists is that the salt layer is thick enough to make this kind of assumptions. Figure 3.6 shows the predicted and extended well used for the wavelet extraction.

The current state of the art of WEB-AVO inversion makes it difficult to invert seismic data with a frequency content that overlaps with the frequency content of the background. The background model is a low frequency model of the log properties filtered with a low-pass filter with full on at 4 Hz and a full of at 6 Hz.

It is difficult to believe that the seismic data in the target interval would have such content on low frequencies. To avoid interaction of the low frequency content with the background, the seismic data has been filtered with a low-cut filter with full-off at 5 Hz and full-on at 10 Hz.

Figure 3.9 shows the results of the seismic to well tie. The panel shows the filtered seismic data, the synthetics matched with the extracted wavelet and a residual. A great amount of time was spent in improving the results of the seismic-to-well match to decrease the residual as much as possible. As explained before, the residual will be used as an estimate of the noise in the data, an important parameter to build the likelihood function. .

Figure 3.10 shows the extracted wavelets, one for every ray-parameter trace in the gather. We noticed that the bandwidth of the wavelet is very narrow. At a great depth, it is normal to have such a lack of high frequencies.

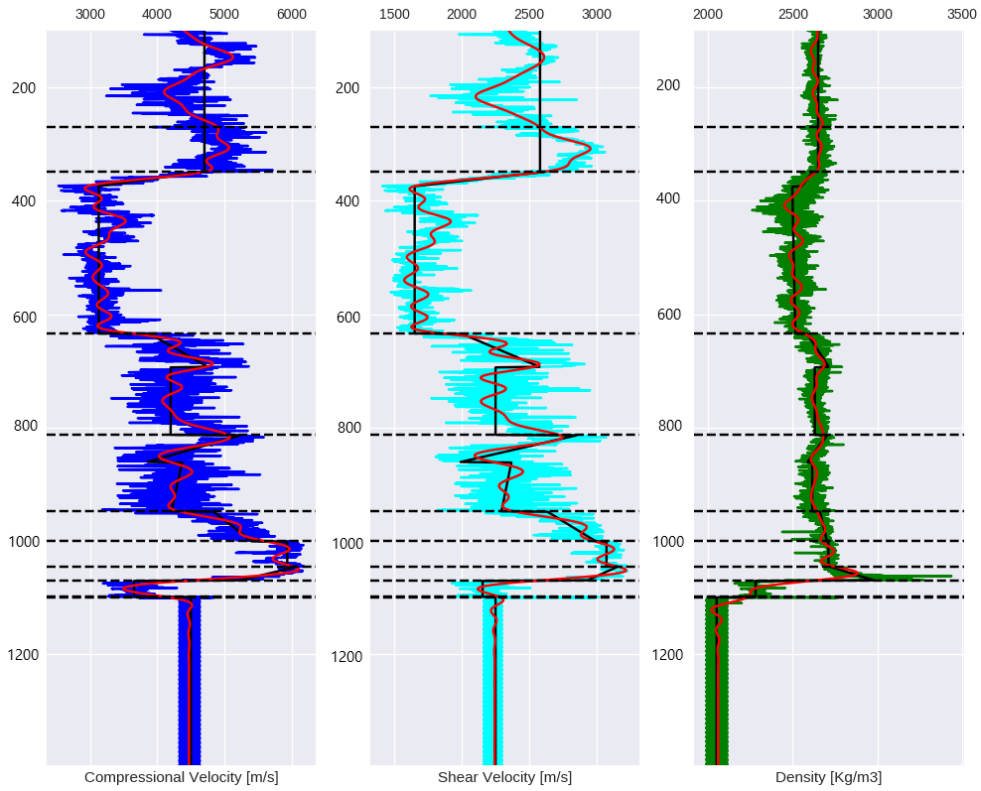

Figure 3.6: Well 2 with predicted values in missing intervals and with a 300 m extension of salt, the red curves are the smooth versions of the logs and the black lines are the interpreted units of the prior.

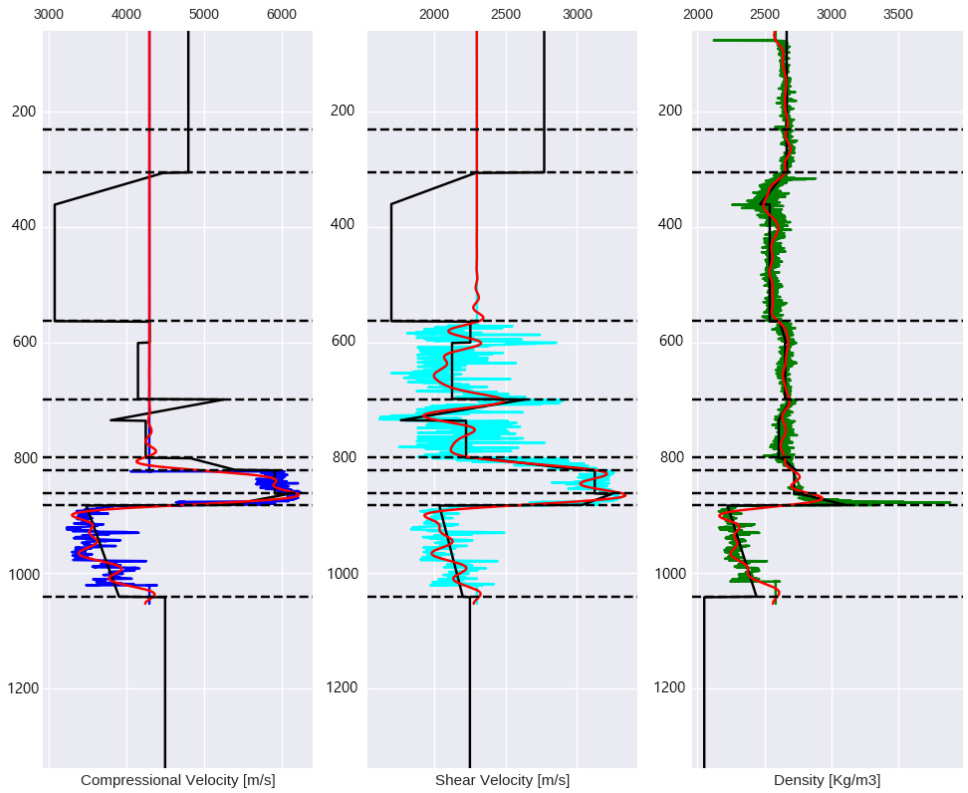

Figure 3.7: Well 1, the red curves are the smooth versions of the logs and the black lines are the interpreted units of the prior.

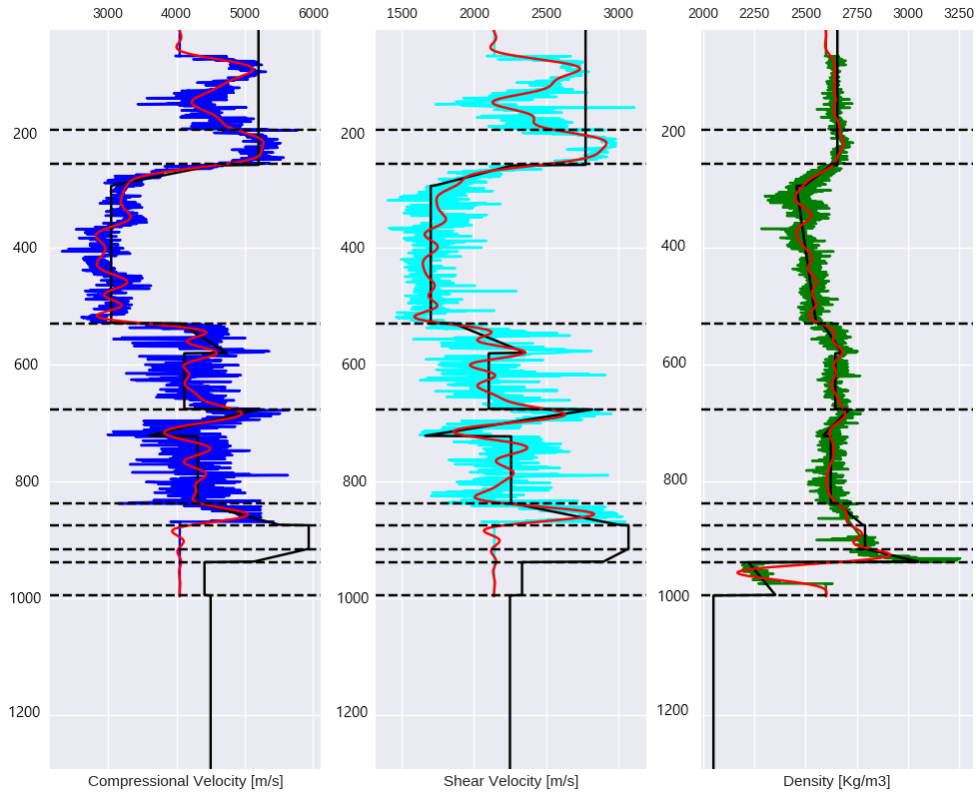

Figure 3.8: Well 3, the red curves are the smooth versions of the logs and the black lines are the interpreted units of the prior.

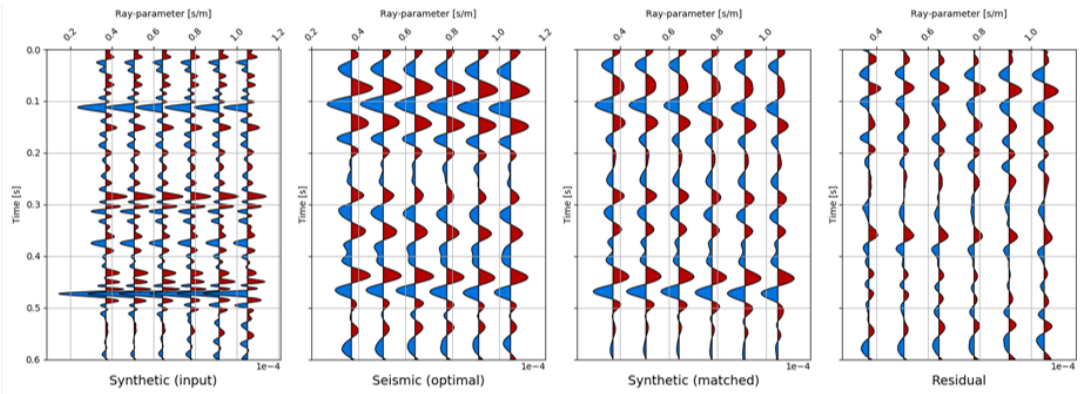

Figure 3.9: Seismic-to-well tie at location of well 2. The panels show the seismic data, the matched Kennett synthetics generated from the smooth logs and the residual.

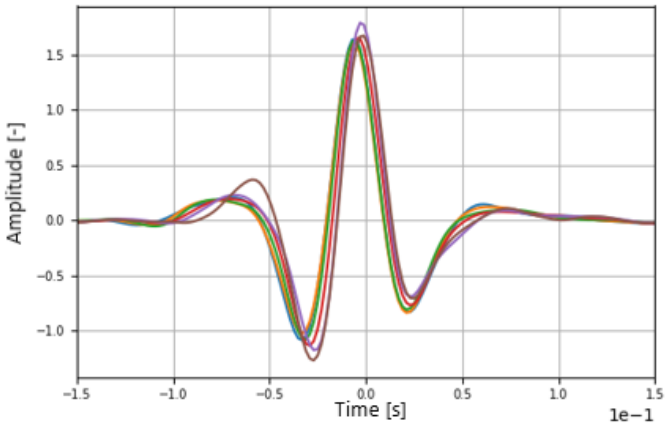

(a) Extracted wavelet in the time domain.

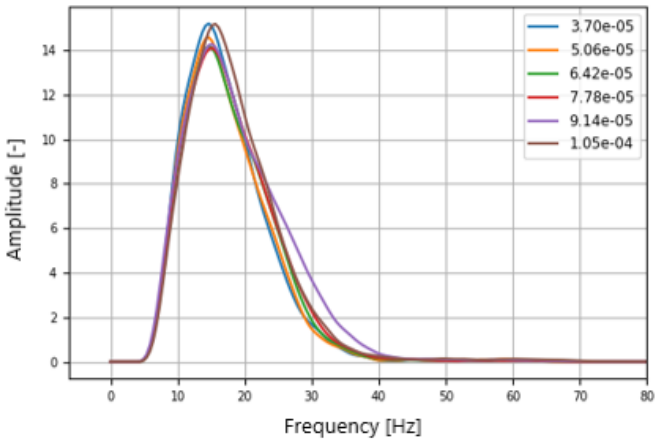

(b) Amplitude spectrum of the extracted wavelet.

Figure 3.10: Result of the seismic-to-well tie.

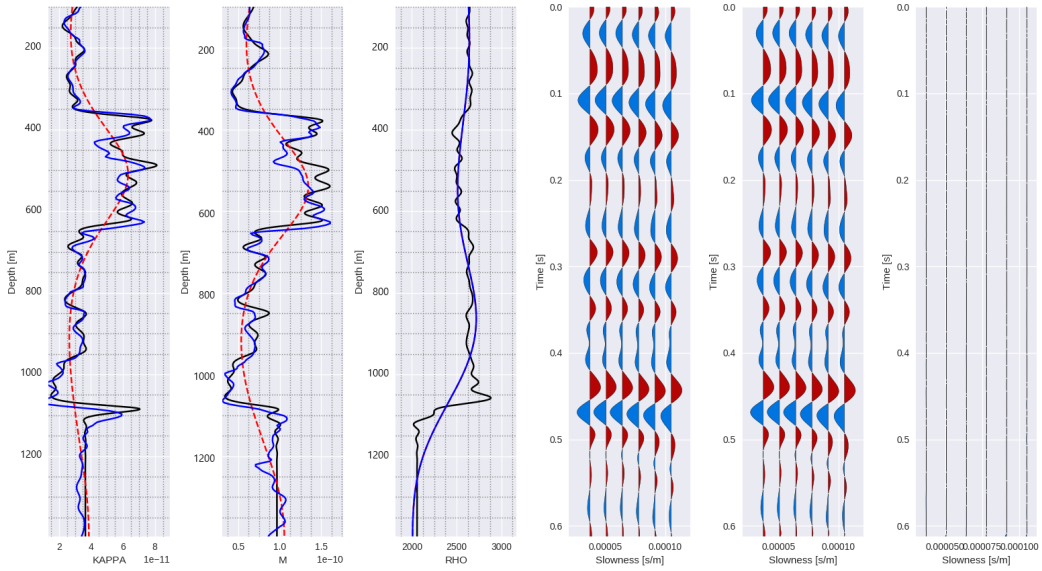

Figure 3.11: WEB-AVO inversion results from Kennett generated synthetic data. The black curves are the smooth true logs, the blue curves are the inverted properties and the red curves are the background. The three panels on the right show the seismic data, the predicted synthetic data based on the inverted parameters and the residual.

For bench-marking purposes, Kennett synthetic data is generated and inverted using the WEB-AVO algorithm. Figure 3.11 shows the result of the inversion of the synthetics. The result of inversion of the synthetic is by definition the best result one could hope to get from inverting the seismic data.

3.4 DETERMINISTIC WEB-AVO INVERSION AT WELL LOCATION

After having obtained optimal results inverting synthetic data, the seismic data has been inverted at the location of well 2. Several parameters have been tested to regularize the result to avoid fitting the noise in the data.

The optimal results were obtained by setting the number of conjugate gradient steps to 5 and by setting the sparse-gradient weight to 0.1. These two parameters control the amount of regularization in the data. Figure 3.12 shows the results of the inversion with different CG steps values and figure 3.13 shows the results of the inversion by varying the sparse weight parameter.

By increasing the number of CG steps in every outer loop iteration, the field update starts to fit the noise in the data and sometimes the results highly diverge from the true values while decreasing the residual. This is the main parameter in place to control regularization. The sparse-gradient weight controls the blockiness of the resulting property values. This parameter plays a minor role in regularizing the result and a lower value is desirable to avoid having a blocky artificial-looking result with possible loss of resolution.

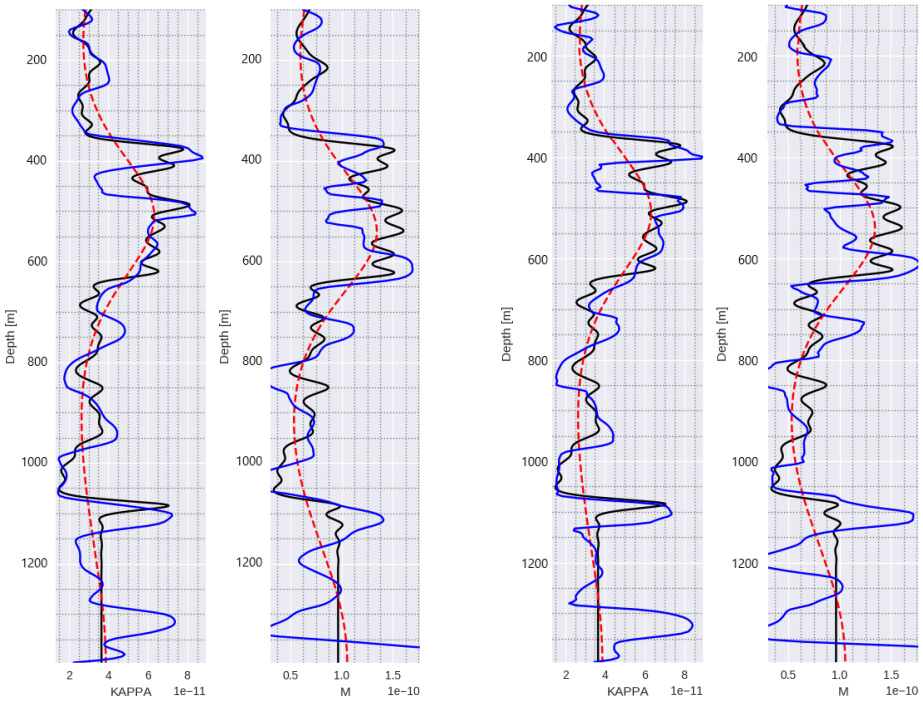

(a) 5 CG steps.

(b) 10 CG steps.

(c) 15 CG steps.

Figure 3.12: Regularization: Compressibility κ issued from inversion of the seismic data with different number of CG steps. The black curves are the smooth true logs, the blue curves are the inverted properties and the red curves are the background.

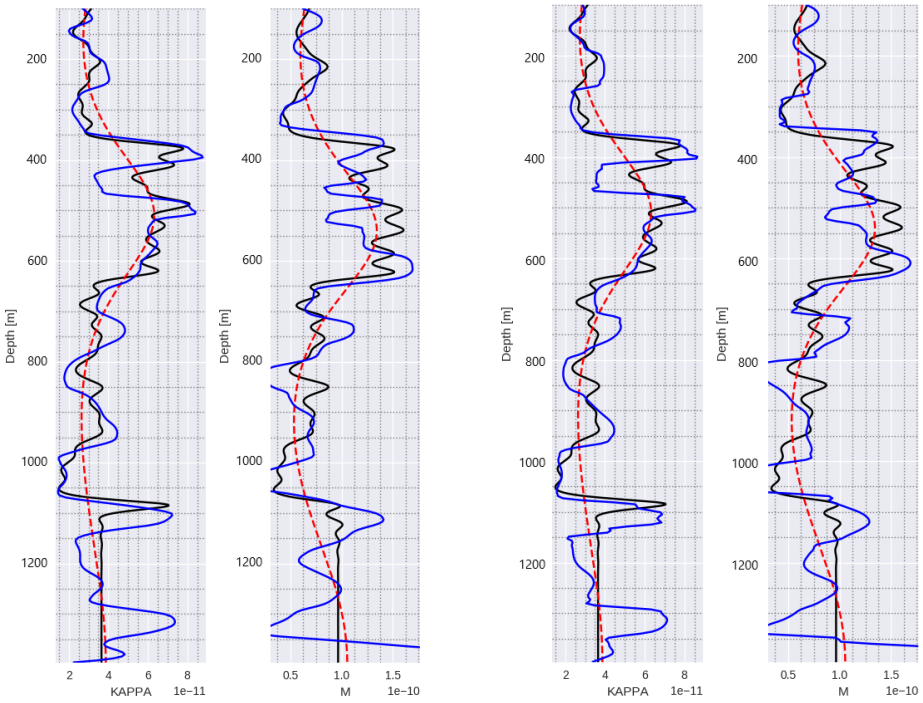

(a) Sparse-gradient weight: 0.1

(b) Sparse-gradient weight: 0.3

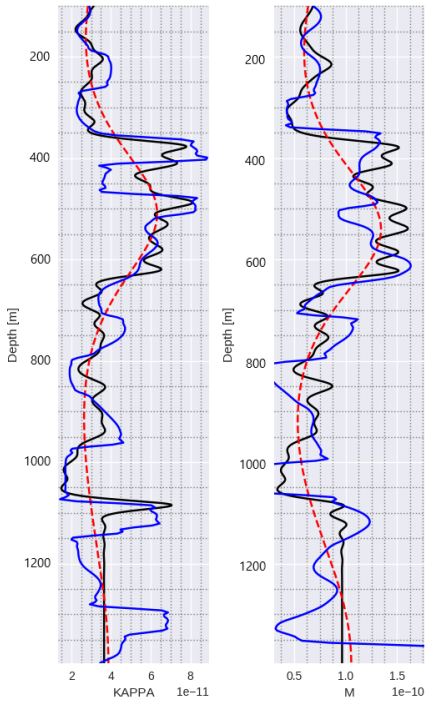

(c) Sparse-gradient weight: 0.5

Figure 3.13: Regularization: Compressibility κ issued from inversion of the seismic data with different sparse gradient weight values. The black curves are the smooth true logs, the blue curves are the inverted properties and the red curves are the background.

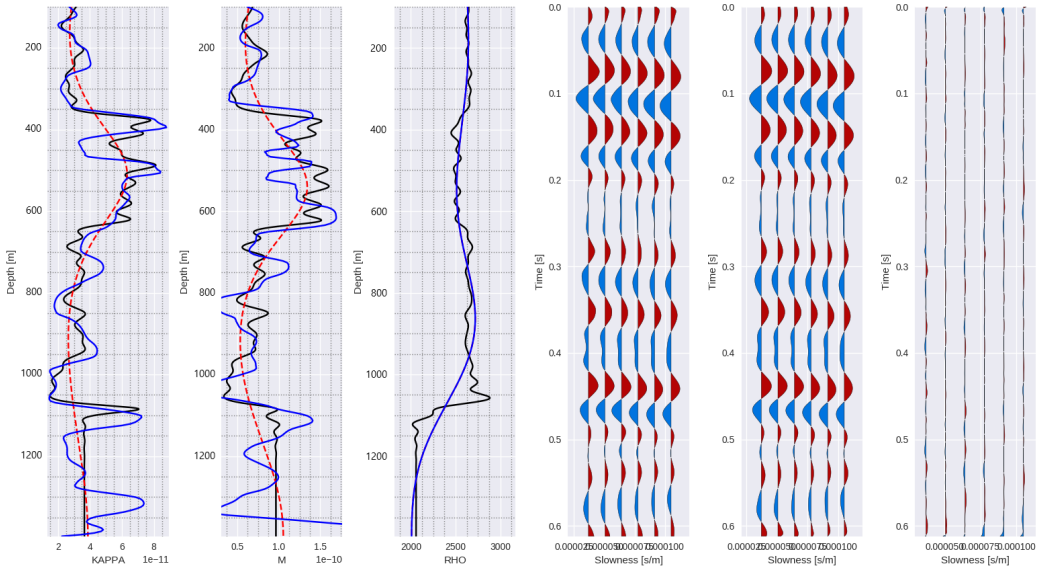

Figure 3.14: WEB-AVO deterministic inversion results from the seismic data at location of well 2. The black curves are the smooth true logs, the blue curves are the inverted properties and the red curves are the background. The three panels of the right show the seismic data, the modelled seismic data with the inverted parameters and the residual.

Another important parameter is the number of field updates the WEB-AVO inversion performs. Every outer loop iteration adds another order of scattering to the total wave-field. Experience from Delft Inversion shows that 20 field updates yield good results. This will be the standard number of outer loop iterations used when inverting the seismic data. Only inversion for compressibility and shear compliance values will be tested (two-parameter inversion).

Figure 3.14 shows the results of the deterministic inversion at the location of well 5 for 2 parameters. Major velocity contrasts at the top of formation C and D are inverted properly and the top of the reservoir layer is nicely reconstructed with a high κ value. Spurious layers are created at the bottom of the sequence at salt level. The seismic data clearly shows events happening inside the layer. However, there is no well information available about what happens inside the salt. The possibility of those events being multiples is also considered.

4 CHAPTER 4: RESULTS AND DISCUSSION

In this section the results of the stochastic inversion will be presented and discussed.

4.1 LIKELIHOOD FUNCTION BUILDING: LOOKING FOR THE NOISE IN THE DATA

Bayes' theorem states that the Posterior probability density function is proportional to the product of the Prior probability density function times the Likelihood function.

In the previous section the creation of the Prior probability density function from well data was discussed, and the Prior was created at the different well locations. The Likelihood function is created from the deterministic results of the WEB-AVO inversion, the m_{mle}. To do that, an estimate of the noise in the data is necessary.

The proposition of the present work is that an accurate estimation of the noise in the data is the residual of the seismic-to-well match. Figure Figure 3.9 shows the residual. Its variance gives a value of 0.01. This value is the σ_N^2 that scales the covariance matrix.

Figures 4.1 shows what happens when the variance changes its value. Intuitively, by setting a smaller variance, e.g. 0.0001, the Likelihood function becomes a very narrow Gaussian like a delta function. Because the starting point for the search for the Maximum A Posteriori (MAP) solution is the MLE estimate, in the case of a very narrow likelihood function the MAP estimate cannot move away from the MLE, and the prior information cannot contribute.

By setting a greater variance, 1, the likelihood function is a wide Gaussian. In this case, the prior will have a great influence on the posterior. In figure fig:fig4.1:3, one observes that some intervals start to behave like the prior, having a constant value.

A trade-off between this two scenarios can be assessed by estimating a realistic value of the noise in the data. Figure 4.1b clearly shows that a variance of 0.01 allows the interaction of the likelihood function with the prior, while maintaining information from the likelihood function.

This parameter can be also modified as a function of the prior knowledge we possess. If one has reasons to trust the seismic data over the prior geological information, a smaller variance can be used. If, on the other hand, one highly trusts the geological information, for example when dealing with very noisy and difficult seismic data, the variance can be increased.

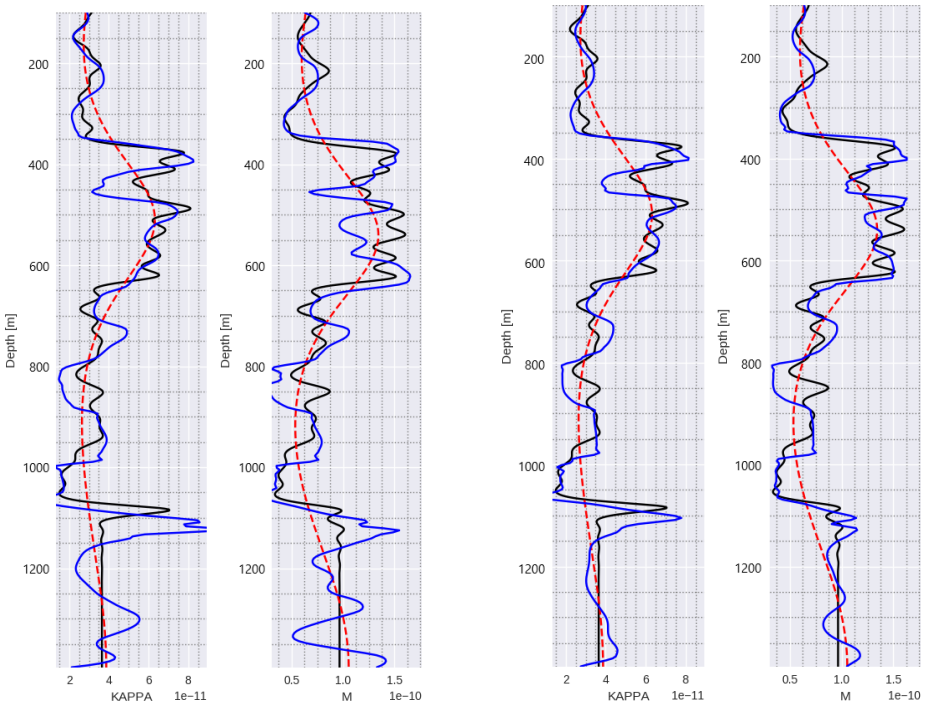

(a) Var = 0.0001

(b) Var = 0.01

(c) Var = 1

Figure 4.1: Stochastic inversion results with different values for the variance of the noise in the data. The black curves are the smooth true logs, the blue curves are the inverted properties and the red curves are the background.

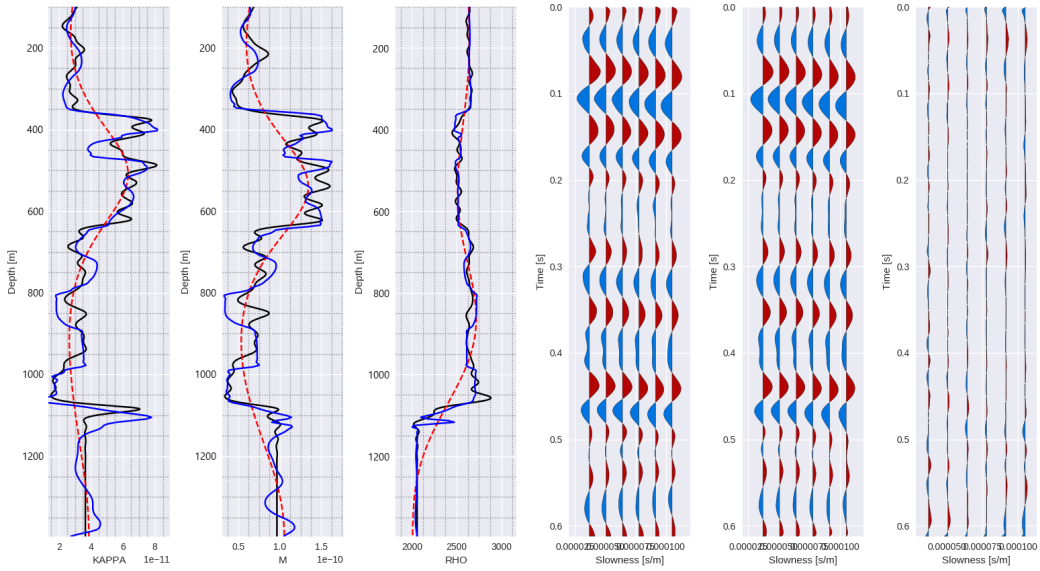

Figure 4.2: WEB-AVO stochastic inversion with optimal parameters and a variance of 0.01. The black curves are the smooth true logs, the blue curves are the inverted properties and the red curves are the background. The three panels on the right show the seismic data, the predicted synthetic data based on the inverted parameters and the residual.

4.2 STOCHASTIC INVERSION AT WELL LOCATIONS

All the ingredients and conditions necessary to perform the stochastic inversion have been discussed and set.

The prior probability density function and the likelihood function are multiplied together to obtain the posterior probability density function at the location of the well 2.

The posterior is a complicated function that we need to maximize (or minimize if we work with the negative of its natural logarithm). A L-BFGS algorithm is used to compute the Maximum a Posteriori estimate (m_{map}), starting from the MLE result. It is a vector that contains the property values for the three parameters κ, M and ρ.

Figure 4.2 shows the results with a variance of 0.01. By bringing prior geological information the WEB-AVO inversion has been further constrained. Using the smoothed well logs as a benchmark, one can observe that the stochastic inversion improves the results in several intervals. The first unit (integrated by formation A and B) and the fourth and fifth unit (formation D) are better predicted.

At reservoir level, one observes that formation I is now thinner. However, the mismatch is not improved, the top of the reservoir is still shifted.

Chaotic events happening at salt level are reduced by the prior. All of this, of course, at the expense of a slight increase in the residual.

Because of the lack of information on Well 1 and 3, a wavelet extraction is difficult without first predicting a great part of the logs.

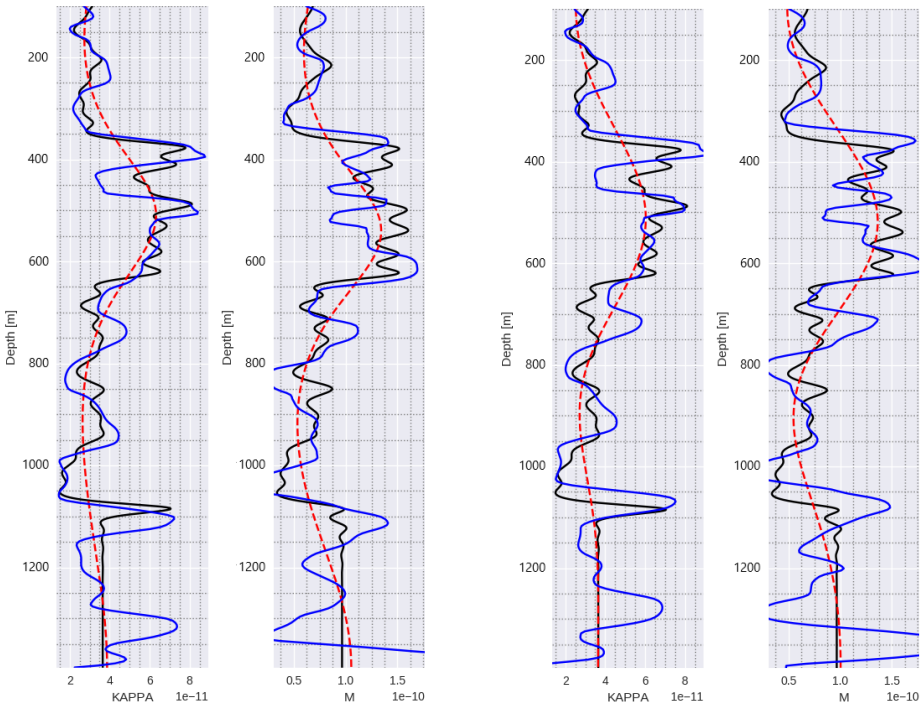

(a) Deterministic inversion results using a background derived from the well logs.

(b) Deterministic inversion results using a background derived from the grid-based mean.

Figure 4.3: Deterministic inversion results comparison between the logs-derived background and the grid-based-derived background. Both background have the same frequency content, a low-ass filter has been applied (4-6 Hz). The black curves are the smooth true logs, the blue curves are the inverted properties and the red curves are the background.

The wavelet extracted at well 2 has been used to invert the whole 2D section. Therefore, at locations near well 2 the best estimates will be obtained. Let's assess the behaviour of the deterministic and the stochastic inversion at the locations of well 1 and well 3. These two locations are the extremes of the 2D section, and they will be the most challenging.

Since the logs are incomplete, a background covering all the target interval cannot be obtained from them. Here, the prior will be useful as well. As mentioned in Chapter 2, the average model of the mixture of Gaussian building the prior will be called the grid-based mean. Such model is our best estimate of the truth when looking at the prior information (thicknesses, property values and standard deviations).

A low-frequency version of the grid-based mean should follow the trend of the log and emulate a background.

Figure 4.3 shows a comparison of the deterministic WEB-AVO inversion using the background derived from the well logs and using the background derived from the grid-based mean. Both backgrounds have been derived by applying a low-pass filter (4-6 Hz) to the well logs and to the grid-based mean respectively. Figure 4.4 shows an equivalent setting but displaying the results of the stochastic inversion.

Both backgrounds, and its resulting property values after inverting the seismic data are similar. Even if overall there is minor discrepancies, at reservoir level there

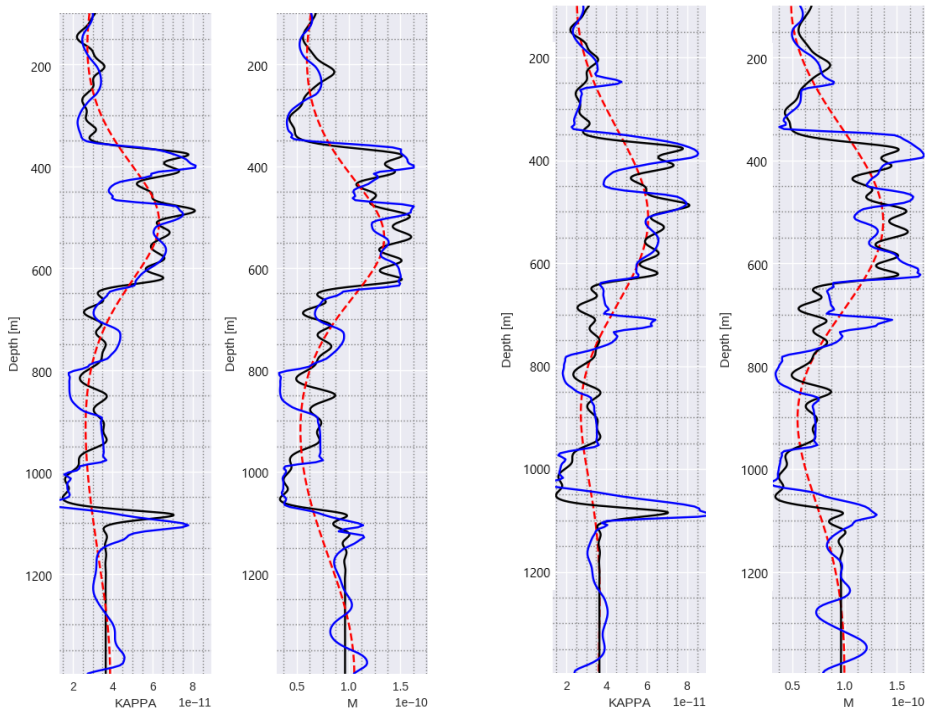

(a) Stochastic inversion results using a background derived from the well logs.

(b) Stochastic inversion results using a background derived from the grid-based mean.

Figure 4.4: Stochastic inversion results comparison between the logs-derived background and the grid-based-derived background. Both backgrounds have the same frequency content, a low-pass filter has been applied (4-6 Hz). The black curves are the smooth true logs, the blue curves are the inverted properties and the red curves are the background.

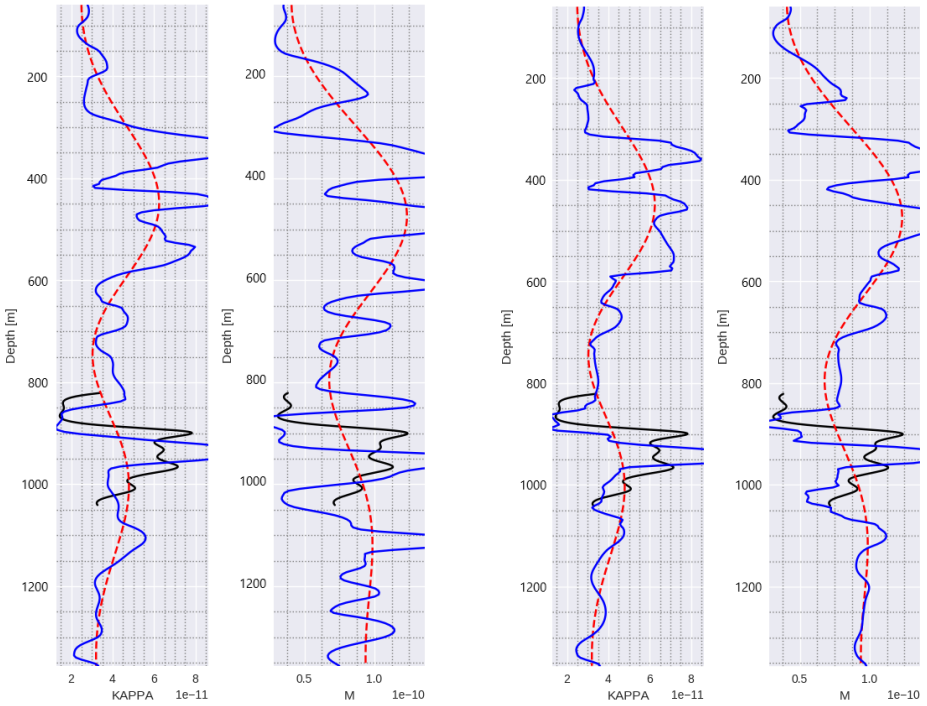

(a) Deterministic inversion results.

(b) Stochastic inversion results.

Figure 4.5: Deterministic and stochastic inversion results comparison at well 1 location using the background derived from the grid-based mean. The black curves are the smooth true logs, the blue curves are the inverted properties and the red curves are the background.

seems to be a shift mismatch in the form of a shift. One needs to keep this in mind when making an interpretation on the other two wells.

For the inversion of seismic data at locations of well 1 and 3, the grid-based mean derived background has been used. Figures 4.5 and 4.6 show the results of the deterministic and stochastic inversions for compressibility and shear compliance at both well locations. The same optimal parameters have been used. One observes in both cases that the property values issued from the inversion are consistent with the overall behaviour but there is mismatch in particular features.

For well 3, benchmarking can be carried out by plotting the upper part of the well. The top of formation C is clearly defined and the variation inside the formation seems to be partially honoured. At the bottom of the well formation I, the reservoir appears with high κ and M values. The MAP estimate seems to be a more constrained result of the inversion. Out of the two properties, M benefits more from the prior by a result that better follows the general trend of the real logs even if many details are missed.

For well 1, the narrow interval where velocities are defined can be plotted for benchmarking. The inversion results are consistent with the results of the other two wells, the top of formations C and D can be easily distinguished. Formation I appears at the right depth, but the thickness is not correct if we compare to the short interval of the well logs. Also, the whole log seems to be shifted towards the bottom. Bringing prior information constrains the inversion results, especially for M. The reservoir top gets closer to its actual depth, but the thickness is never fully recovered.

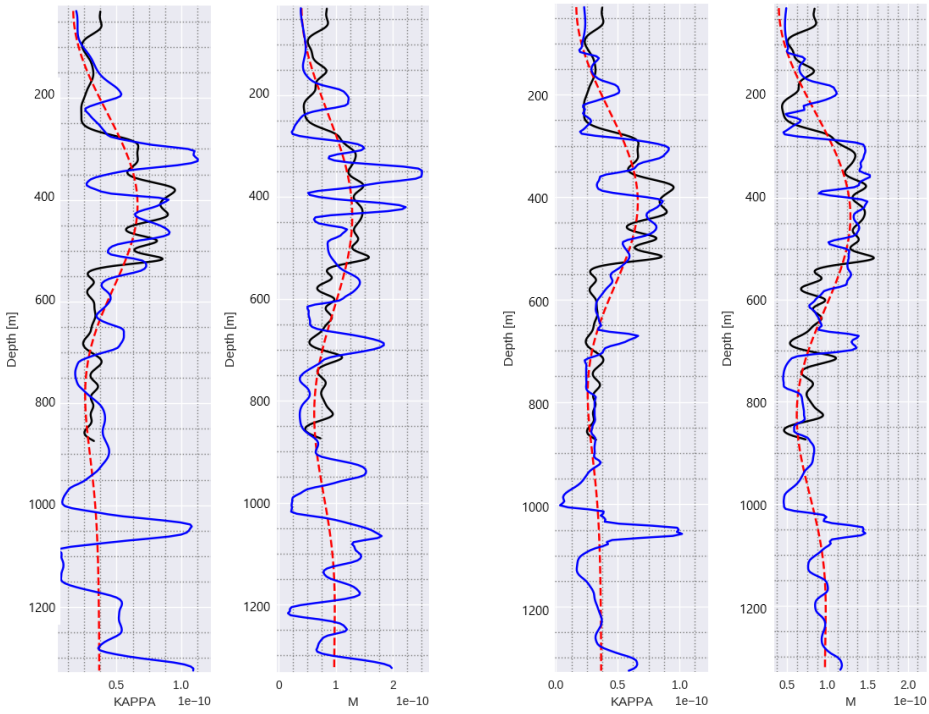

(a) Deterministic inversion results.

(b) Stochastic inversion results.

Figure 4.6: Deterministic and Stochastic inversion results comparison at well 3 location using the background derived from the grid-based mean. The black curves are the smooth true logs, the blue curves are the inverted properties and the red curves are the background.

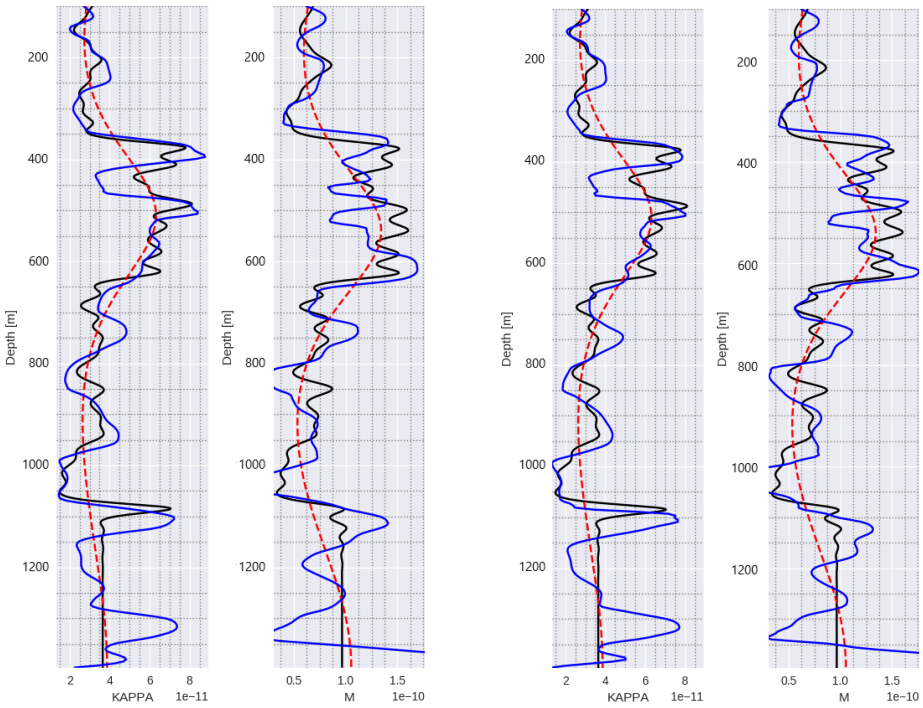

(a) Background as starting model.

(b) Grid-based mean used as a starting model.

Figure 4.7: Deterministic inversion results that compare the use of the background starting model vs using the grid-base mean as a starting model at well two location.

In a nutshell, the stochastic inversion constrains the result of the three wells towards the real values by bringing prior geological information. Since we lack information at location 1 and 3, a background created from the grid-based mean can be used.

4.3 STOCHASTIC INVERSION USING GRID-BASED MEAN AS STARTING MODEL

The WEB-AVO inversion starts its first field iteration, either with the background itself, or with a meaningful starting model derived from the prior information.

It has been long discussed that the grid-based mean is the average of a mixture of Gaussians that contains information about the thickness, property values and its respective standard deviations. The grid-based mean is the best non-biased estimate of the truth that the prior can yield. The grid-based mean can therefore be used as a starting model of the WEB-AVO inversion.

Figures 4.7 and 4.8show the deterministic and stochastic results of the WEB-AVO inversion using the grid-based mean as a starting model at well 2 location.

We see some minor improvements in certain areas where the inverted values get closer to the truth. The local grid-based mean will be therefore used as a starting model for every location.

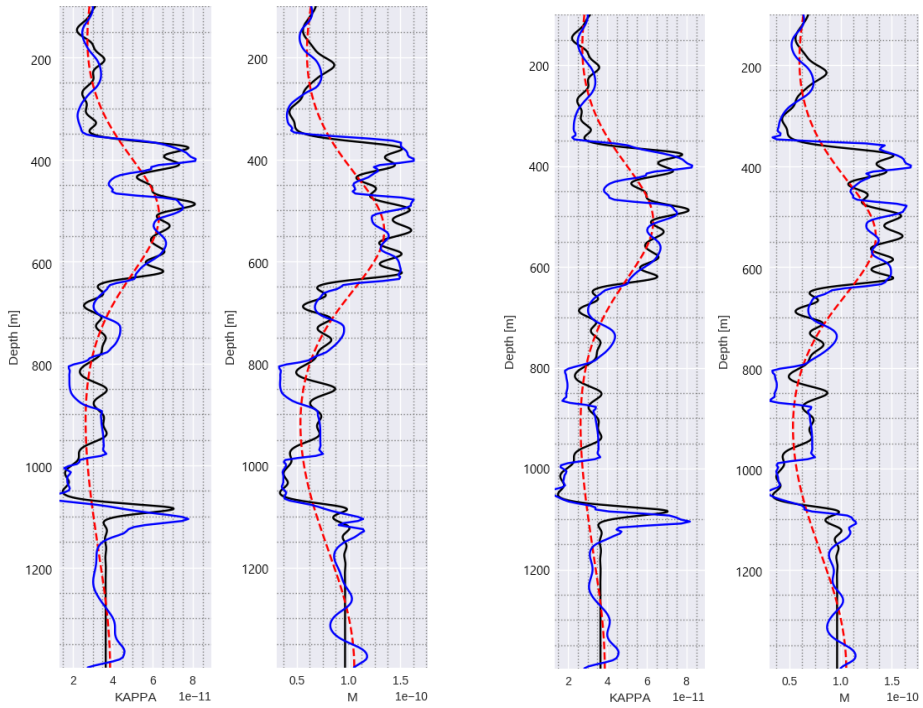

(a) Background used as starting model.

(b) Grid-based mean used as a starting model.

Figure 4.8: Stochastic inversion results that compare the use of the background as starting model vs using the grid-base mean as a starting model at well 2 location.

4.4 RANDOM REALISATIONS

When we look at the stochastic inversion of the 2D seismic section, it is important to realise that by computing the second derivative of the posterior probability density function at the MAP location, one can estimate the variances of the posterior.

The present project aims to assess a second source of uncertainty inherent to the WEB-AVO inversion, the intrinsic uncertainty, or the non-uniqueness, of the method. The method itself has its limitations when obtaining property values from seismic properties. To prove this point and assess the amount of uncertainty, 100 random realisations, drawn from the prior distribution, are used as the starting model for the inversion. For the sake of this assessment, the synthetic data is used for the inversion. A perfect and controlled data set must be used to avoid assessing other sources of uncertainty

A random realisation is a sample drawn from the prior and used as the starting model for the WEB-AVO inversion. The most optimistic scenario would be that for every single starting model the same inversion result is obtained.

This scenario would mean that the inversion has a unique solution and is, therefore, insensitive to the starting model.

This is of course not the case. Figure 4.9 shows histograms of the random input realisations for several grid-points. The histograms capture the non-Gaussian and complex behaviour of the prior probability function, from which these realisation were drawn.

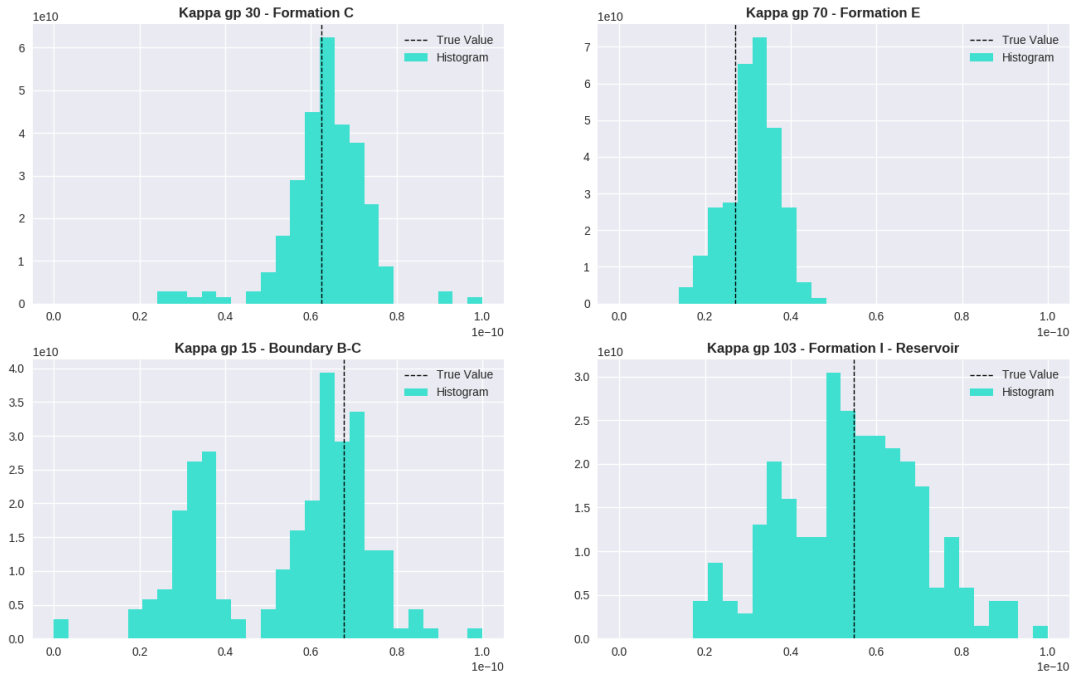

Figure 4.9: Histograms for four κ grid-points for 100 random realisation sampled from the prior.

Figure 4.10 shows the histograms for the values of the same grid-points but after the WEB-AVO inversion without posterior update. The result for every grid-point is a Gaussian distribution, which means that there is an intrinsic non-uniqueness in the inversion method. This uncertainty can even be different for every single grid-point as observed in the histograms. Grid-point 103 belonging to formation I has a greater intrinsic uncertainty than grid-point 15 located at the interface between formations B and C.

The variances and covariances between properties for every single grid-point can be computed. In order to obtain the full uncertainty of the inversion results, the property covariance matrix due to non-uniqueness of the inversion can be added to the covariance matrix of the Likelihood function in case we do not perform a posterior update, or to the covariance of the posterior distribution function in case we do perform a posterior update.

In principle, a pure stochastic approach to the inversion using the prior would be to draw a great number of random realisations, use them as starting models for the inversion, and take the average model as the result, with, or without posterior update. This approach is computationally very expensive. Figure 4.11 compares the MAP estimate of a synthetic run on well 2 versus the mean of the random realisations for every grid-point. They are both similar, but the MAP update seems to do a better job in approximating the true logs. An important remark to make is that the MAP update, when properly implemented, is computationally cheaper, one does not need to run the inversion multiple times using the random realisations as starting models. The same figure shows a green curve which is the standard deviation computed from the random realisations for every grid-point, i.e. the intrinsic uncertainty in the method.

Figure 4.12 shows the uncertainty assessment of inversion of the seismic data. The results of the stochastic inversion (MAP) are plotted next to the true smooth logs at the location of well 2. By computing the second derivative of the posterior distribution for the MAP estimate, an estimate is obtained of the uncertainty of the

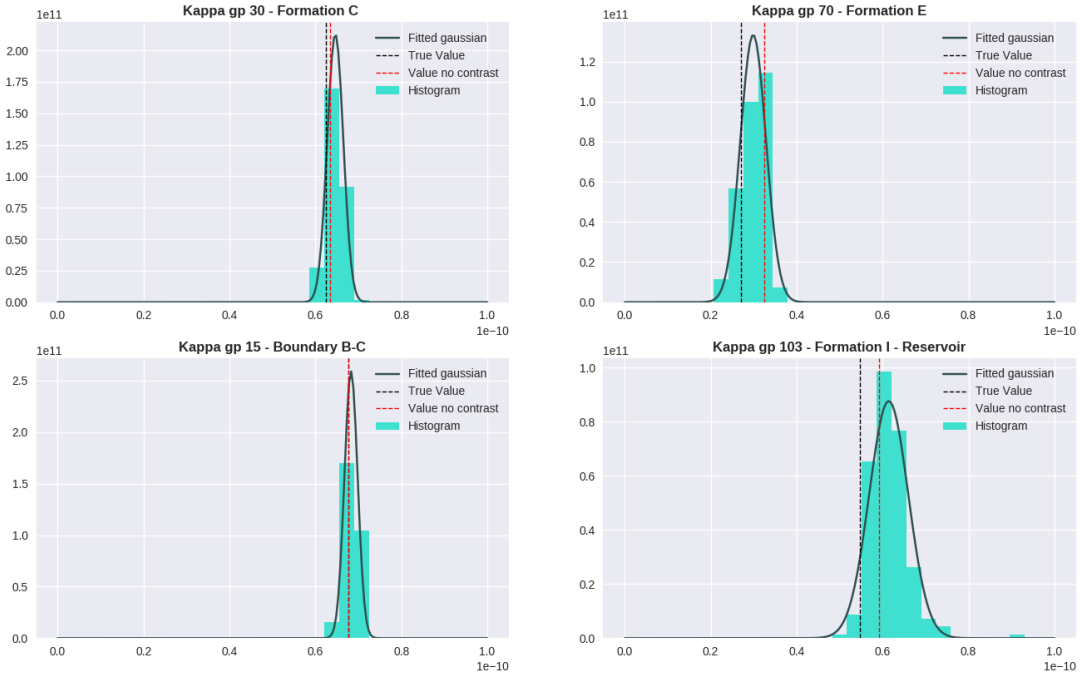

Figure 4.10: Histograms of the inversion results using the 100 random realisations as the starting model. The 'True value' is the grid-point value from the smooth wells and the 'Value no contrast' is the result of the inversion using the background as starting model.

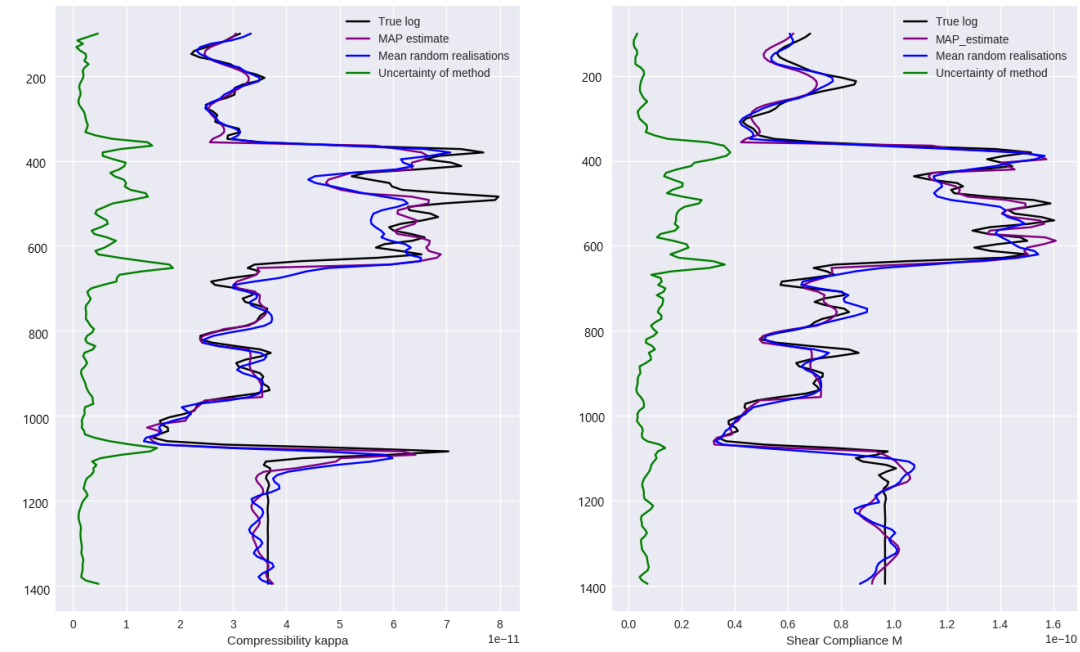

Figure 4.11: Assessment of the uncertainty of the inversion method on synthetic data. The green curve is the standard deviation computed from the random realisations for every grip-point.

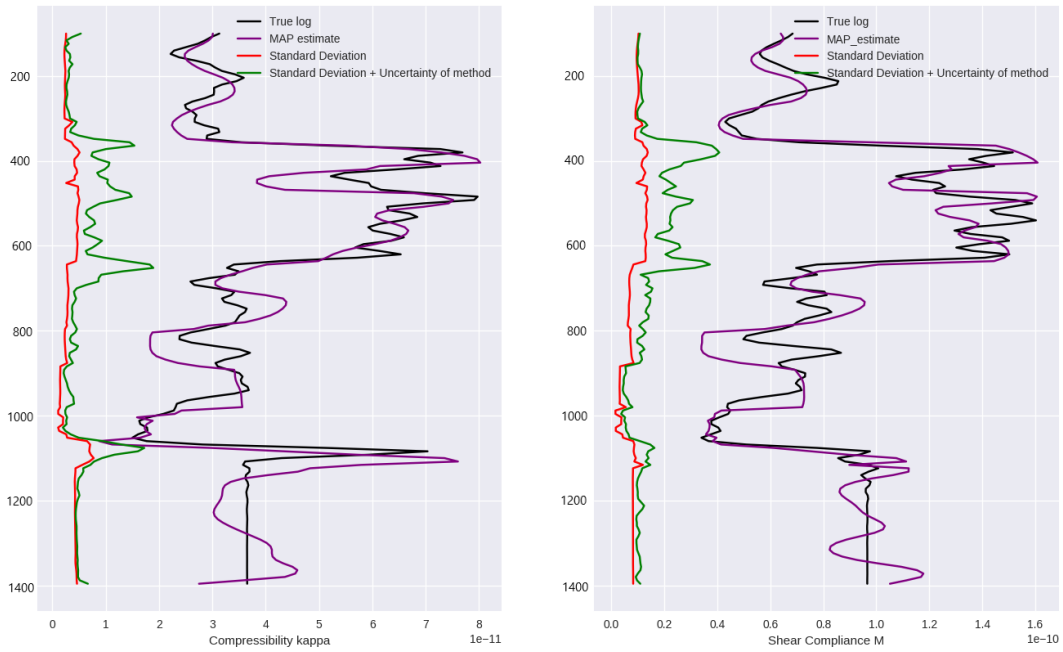

Figure 4.12: Assessment of the global uncertainty incorporating the uncertainty of the inversion in the seismic data. The green curve is now the uncertainty estimated from the posterior and it incorporates the uncertainty of the method.

inversion result due to the width of the posterior distribution, which is strongly affected by the estimate of the noise in the data. This information is the covariance matrix of the posterior. The red curve is the standard deviation derived from this covariance matrix. By combining the uncertainty due to noise in the data and the uncertainty due to intrinsic non-uniqueness in the method, the green curve is obtained, which represents the square root of the sum of the variances of the posterior and of the intrinsic uncertainty. The new estimate is a true measure of the total uncertainty of the inversion. By comparing all the curves it is clear that the error defined by the green curve is a much more realistic estimate of the actual prediction errors of the MAP estimate against the truth.

4.5 2D SECTION DETERMINISTIC AND STOCHASTIC INVERSION

The 2D arbitrary line connecting wells 1, 2 and 3 was selected to be inverted and images for κ and M were created. The three wells are all deviated, for the purpose of selecting the point where the section intersects the well tracks, the reservoir level has been chosen for all three wells.

The section was divided into 78 equidistant locations 30 meters apart. The total length covered is 2360 m. Well 1 is located on one extreme of the section and well 3 is located on the opposite extreme. Well 2 is located close to location 31.

The seismic data of the section has received the same pre-processing described during the seismic-to-well tie. A window of 800 ms has been extracted. The interpreted horizon of the top of formation C is very consistent, and consequently, the start of the window follows the same horizon iso-packed 100 ms upwards.

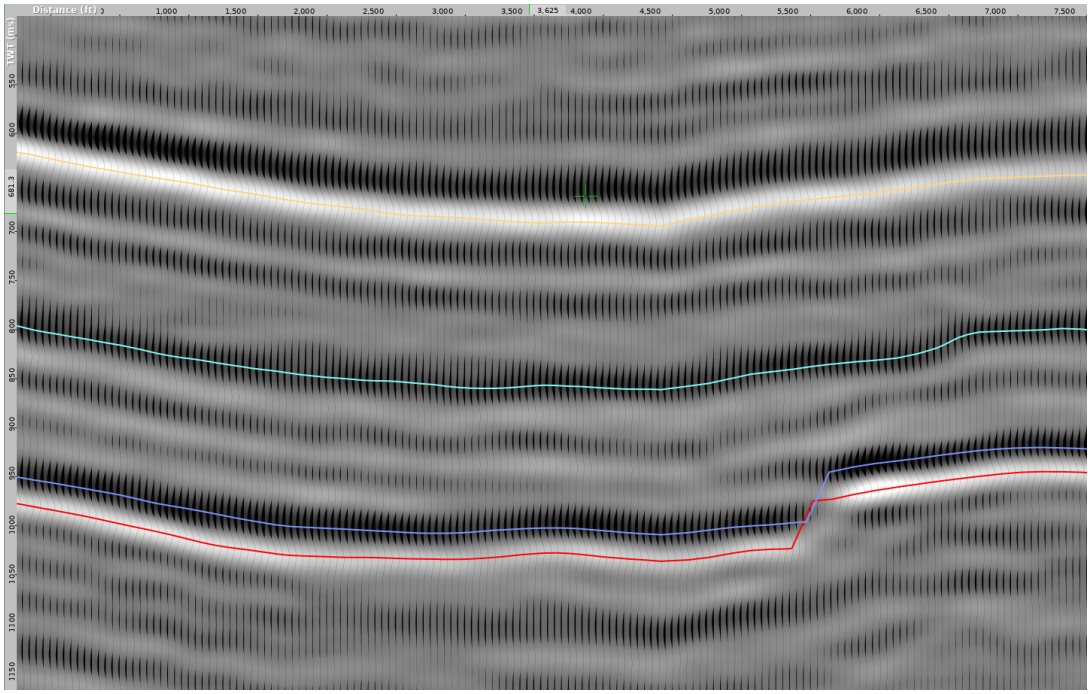

Figure 4.13: Near offset of the 2D section. Well 3 is located at the extreme left and well 1 is located at the extreme right.

The near-offset seismic section can be seen in figure 4.13. It is important to point out that between well 1 and well 2 a fault is present. The seismic data between well 2 and well 3 is consistent and it follows the same horizontal trend with well defined horizons. The yellow horizon is the top of formation C, the cyan horizon is the top of formation D, the blue horizon is the top of formation G, and the red curve is the top of formation I, the top of the reservoir.

Figure 4.14 shows the colour maps for the κ and M results of the deterministic WEB-AVO inversion. Figure 4.15 shows the results of the stochastic WEB -AVO inversion. One can immediately observe that some layers are better defined, and some anomalies have been removed.

The fault is a feature that looks well defined even without the prior and is well preserved by the MAP update.

For both κ and M high values are obtained for small section of the 2-D map. By bringing prior information, the inversion is better constrained, and these high values decrease. A clear example are the events happening at the salt layer level. The events are greatly diminished. It is important to point out that the prior is a complex function that involves several parameters, so, the result of the inversion is an optimized set of property values that involve both the information in the deterministic inversion and the information in the prior.

There are some areas where the stochastic inversion seems to behave poorly compared to the deterministic inversion. at location 67 around 6700 ms, some anomalies are created which appear to be artefacts.

At reservoir level, the definition of formations H and I seems to be better constrained.

We already discussed in relation to the examples seen in previous sections that M seems to benefit more from the prior thank κ. The deterministic inversion results for M yield a poor definition of the boundaries of formations H and I. The prior better

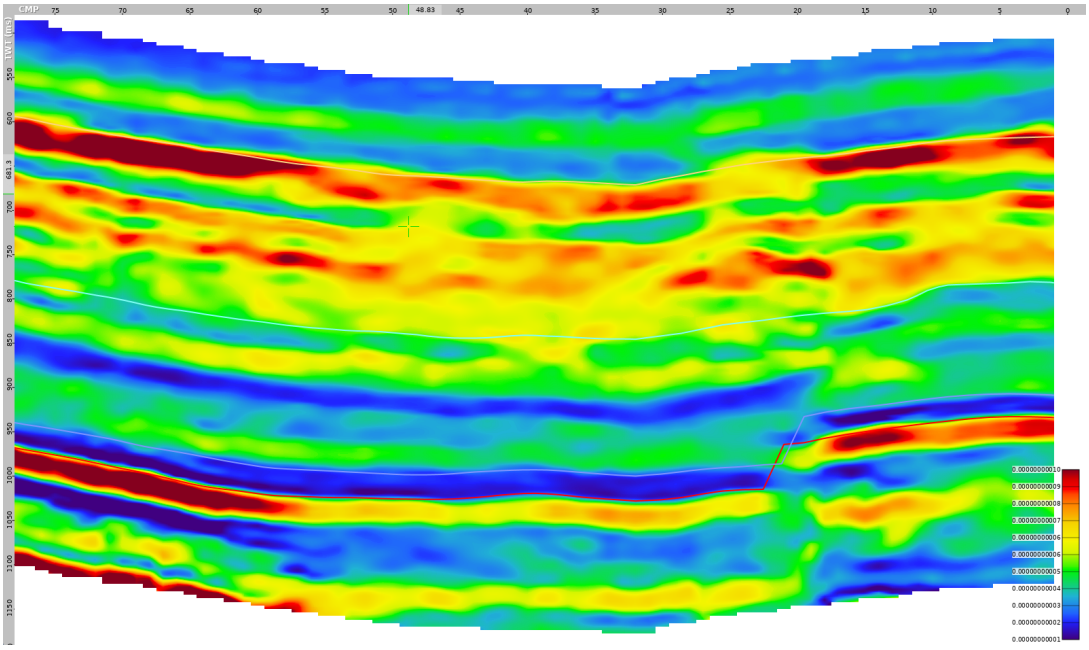

(a) Deterministic Inversion.

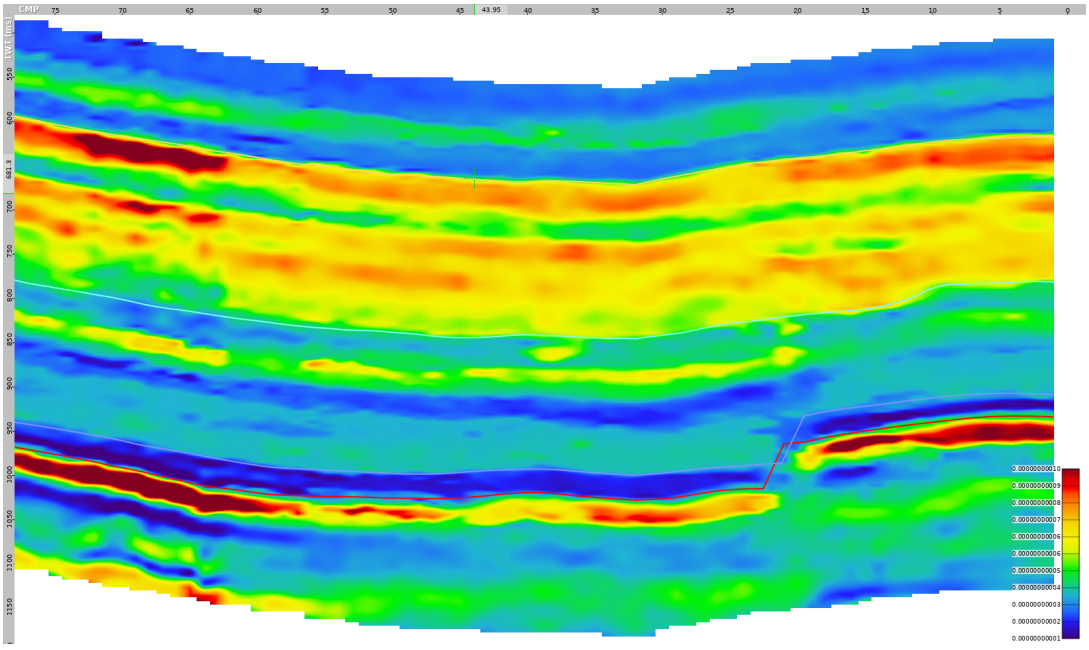

(b) Stochastic Inversion.

Figure 4.14: Comparison of deterministic inversion vs stochastic inversion for κ over the 2D line going from well 3 to well 2 and from well 2 to well 1. The units are m^2/N.

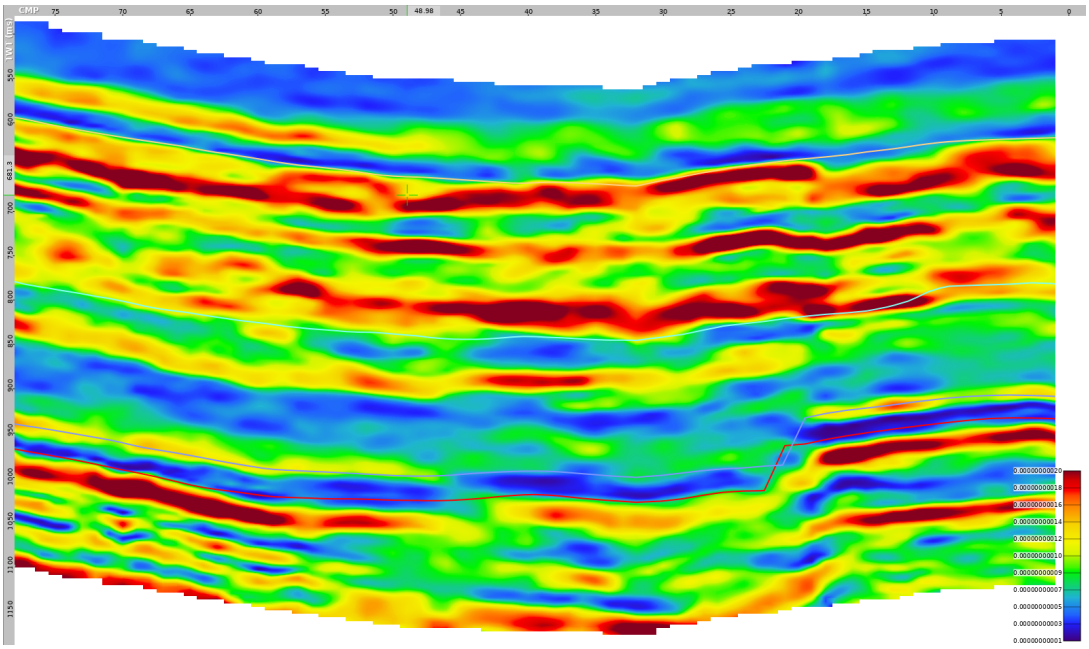

(a) Deterministic Inversion.

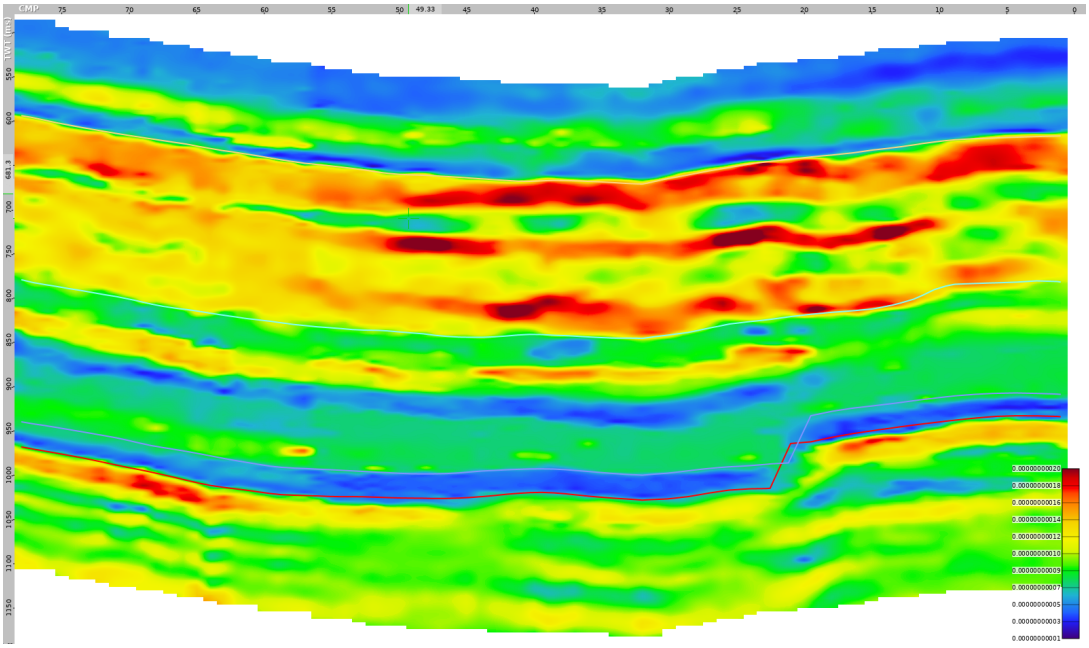

(b) Stochastic Inversion.

Figure 4.15: Comparison of deterministic inversion vs stochastic inversion for M over the 2D line going from well 3 to well 2 and from well 2 to well 1. The units are m^2/N.

constrains the inversion and both formation are better captured by the stochastic inversion.

5 CONCLUSIONS

Stochastic inversion uses Bayes' theorem to incorporate prior geological information obtained from well logs and seismic horizons, into the WEB-AVO inversion. A real case study has been used to work on and to assess the stochastic inversion results.

The prior probability density function is a mixture of multi-variate Gaussians incorporating information on the thickness of the layers, property values and their corresponding standard deviations. A layer-based model is transformed to a grid-based model (compatible with the inversion structure) by building a weight matrix from all layer thickness distributions.

The likelihood function is built from the results of the deterministic WEB-AVO inversion. The function is assumed to be Gaussian and the covariance matrix is scaled by a factor representative of the noise in the data.

The likelihood function is multiplied by the prior function, creating a posterior distribution which is optimized to find the Maximum a Posteriori estimate.

The present work has proposed to use the residual of the seismic-to-well tie as the best estimate of the noise in the data. It has been proven in the present work that the variance of the residual of the seismic-to-well match ensures a fair trade-off between weighting the prior function and weighting the likelihood function.

The second source of uncertainty assessed in the present work is the intrinsic uncertainty of the method due to non-uniqueness. By drawing random realisations from the prior and using them as starting models for the WEB-AVO inversion, with, or without MAP updates, the intrinsic uncertainty for every grid-point can be quantified. The variance of the inversion results for every random realisation is added to the variance of the posterior. This is a more accurate estimation of the whole uncertainty of the inversion.

The study case presented in the present work is a challenging setting where a reservoir is obscured by a hard layer that reflects a lot of the energy and creates internal multiples and mode-conversions. In principle this can be handled by WEB-AVO. By further constraining the inversion using prior geological information, the stochastic WEB-AVO inversion yielded a geologically constrained result. High anomalous values decrease, and certain boundaries are better defined. M seems to improve significantly more from stochastic inversion than κ.

By properly assessing the sources of uncertainty, the stochastic WEB-AVO inversion is a method that can lead to a general improvement of the inversion results by incorporating geological information interpreted from wells, while keeping track of the uncertainty of the predictions.

BIBLIOGRAPHY

Asquith, G. and Krygowski, D. (2004). *Basic Well Log Analysis*. AAPG, Tulsa.

Barajas-Olalde, C., Haffinger, P., Gisolf, D., Zhang, M., Droujinina, A., Doulgeris, P., Khatibi, S., Jin, L., Burnison, S. A., Hamling, J. A., and Gorecki, C. D. (2019). *Simultaneous time-lapse WEB-AVO inversion for seismic reservoir monitoring: Application to CO2 enhanced oil recovery at the Bell Creek oil field*, pages 564–568.

Bayes, T. (1763). Lii. an essay towards solving a problem in the doctrine of chances. by the late rev. mr. bayes, f. r. s. communicated by mr. price, in a letter to john canton, a. m. f. r. s. *Philosophical Transactions of the Royal Society of London*, 53:370–418.

Beller, M., Doulgeris, P., Gisolf, A., Haffinger, P., Huis in't Veld, R., and Wever, A. (2015). Resolving carboniferous stacked channel sequences with a non-linear avo technology. 2015(1):1–5.

Buland, A. and Omre, H. (2003). Bayesian linearized avo inversion. *Geophysics*, 68(1):185–198.

Claerbout, J. F. (1985). *Imaging the Earth's Interior*. Blackwell Scientific Publications, Ltd., GBR.

Contreras, A., Gerhardt, A., Spaans, P., and Docherty, M. (2019). *AVA deterministic, stochastic and wave-equation based seismic inversion for the characterization of fluvio-deltaic gas reservoirs of Western Australia*, pages 3185–3189.

Dhelie, P., Danielsen, V., Straith, K., Ndingwan, A. O., Droujinina, A., Doulgeris, P., Gisolf, D., Haffinger, P., Zhang, M., and Mannini, A. (2019). Lithology estimation at the edvard grieg field using wave-equation based seismic avo inversion. 2019(1):1–5.

Fichtner, A. (2019). *Fundamentals of Modern Inverse Theory: Course notes*. ETH Zurich.

Gisolf, A. (2016). Parameterisation for reservoir oriented avo inversion. In *78th EAGE Conference and Exhibition 2016: Efficient Use of Technology - Unlocking Potential*. EAGE. 78th EAGE Conference and Exhibition 2016: Efficient Use of Technology - Unlocking Potential ; Conference date: 30-05-2016 Through 02-06-2016.

Gisolf, A. and M. van den Berg, P. (2010). Target oriented non-linear inversion of seismic data.

Gisolf, A. and Van den Berg, P. (2012). Target-oriented elastic full wave form inversion. 74th EAGE Conference and Exhibition.

Gisolf, D., Haffinger, P. R., and Doulgeris, P. (2017). Reservoir-oriented wave-equation-based seismic amplitude variation with offset inversion. *Interpretation*, 5(3):SL43–SL56.

Gisolf, D. and Verschuur, E. (2010). *The principles of quantitative acoustical imaging*. EAGE Publ.

Haffinger, P., Eyvazi, F. J., Steeghs, P., Doulgeris, P., Gisolf, D., and Verschuur, E. (2018). Quantitative prediction of injected co2 at sleipner using wave-equation based avo. 2018(1):1–5.

Haffinger, P., von Wussow, P., Doulgeris, P., Henke, C., and Gisolf, A. (2015). Reservoir delineation by applying a nonlinear avo technique - a case study in the nile delta. 2015(1):1–5.

Joyce, J. (2019). Bayes' theorem. In Zalta, E. N., editor, *The Stanford Encyclopedia of Philosophy*. Metaphysics Research Lab, Stanford University, spring 2019 edition.

Kearey, P., Brooks, M., and Hill, I. (2002). *An Introduction to Geophysical Exploration*. Blackwell Science, Oxford.

Kennett, B. L. N. (1979). Theoretical reflection seismograms for elastic media*. *Geophysical Prospecting*, 27(2):301–321.

Liner, C. L. (2016). *Elements of 3D Seismology, Third edition*. Society of Exploration Geophysicists.

Liu, D. and Nocedal, J. (1989). On the limited memory bfgs method for large scale optimization. *Mathematical Programming*, 45:503–528.

Oliver, D. S., Reynolds, A. C., and Liu, N. (2008). *Inverse Theory for Petroleum Reservoir Characterization and History Matching*. Cambridge University Press.

Pratt, R. G. (1999). Seismic waveform inversion in the frequency domain, part 1: Theory and verification in a physical scale model. *Geophysics*, 64:888–901.

Russell, B. H. (1988). *2. Part 2 - The Convolutional Model: Course Notes Series*. Society of Exploration Geophysicists.

Scales, J. and Tenorio, L. (2001). Prior information and uncertainty in inverse problems. *Geophysics*, 66.

Sharma, S. (2019). *Honouring Geological Information in Seismic Amplitude-Versus-Slowness Inversion A Bayesian Formulation for Integrating Seismic Data and Prior Geological Information*. PhD thesis, Delft University of Technology.

Sheriff, R. E. (2002). *Encyclopedic Dictionary of Applied Geophysics*. Society of Exploration Geophysicists.

Tarantola, A. (1984). Linearized inversion of seismic reflection data*. *Geophysical Prospecting*, 32(6):998–1015.

Virieux, J. and Operto, S. (2009). An overview of full-waveform inversion in exploration geophysics. *Geophysics*, 74.

Walther, J. (1894). Einleitung in die geologie als historische wissenschaft. in lithogenesis der gegenwart. *Jena: G. Fischer*, 3:535–105.

COLOPHON

This document was typeset using LaTeX. The document layout was generated using the arsclassica package by Lorenzo Pantieri, which is an adaption of the original classicthesis package from André Miede.